UNIVERSIDADE FEDERAL DE PERNAMBUCO
DEPARTAMENTO DE FÍSICA – CCEN
PROGRAMA DE PÓS-GRADUAÇÃO EM FÍSICA

RAFAEL MAGALHÃES JUNGMANN

MELTING PROCESSES OF TWO DIMENSIONAL CONFINED COLLOIDS INTERACTING VIA A QUASI-SQUARE WELL POTENTIAL

Recife
2018

RAFAEL MAGALHÃES JUNGMANN

MELTING PROCESSES OF TWO DIMENSIONAL CONFINED COLLOIDS INTERACTING VIA A QUASI-SQUARE WELL POTENTIAL

Dissertação apresentada ao Programa de Pós-Graduação em Física da Universidade Federal de Pernambuco, como requisito parcial para a obtenção do título de Mestre em Física.

Área de concentração: Física Teórica e Computacional

Orientador: Prof. Dr. Sérgio Wlademir da Silva Apolinário

Recife

2018

Catalogação na fonte
Bibliotecária Elaine Freitas CRB4-1790

J95m Jungmann, Rafael Magalhães
Melting processes of two dimensional confined colloids interacting via a quasi-square well potential / Rafael Magalhães Jungmann. – 2018.
72 f. : fig., tab.

Orientador: Sérgio Wlademir da Silva Apolinário
Dissertação (Mestrado) – Universidade Federal de Pernambuco. CCEN. Fisica. Recife, 2018.
Inclui referências.

1. Dinâmica Molecular 2. Interações Competitivas 3. Física Teórica I. Apolinário, Sérgio Wlademir da Silva (Orientador) II. Título.

530 CDD (22. ed.) UFPE-FQ 2018-50

RAFAEL MAGALHÃES JUNGMANN

MELTING PROCESSES OF TWO DIMENSIONAL CONFINED COLLOIDS INTERACTING VIA A QUASI-SQUARE WELL POTENTIAL

Dissertação apresentada ao Programa de Pós-Graduação em Física da Universidade Federal de Pernambuco, como requisito parcial para a obtenção do título de Mestre em Física.

Aprovada em: 09/07/2018.

BANCA EXAMINADORA

_____

Prof. Dr. Sérgio Wlademir da Silva Apolinário
Orientador
Universidade Federal de Pernambuco

_____

Prof. Dr. Maurício Domingues Coutinho Filho
Examinador Interno
Universidade Federal de Pernambuco

_____

Prof. Dr. Fernando Jorge Sampaio Moraes
Examinador Externo
Universidade Federal Rural de Pernambuco

ACKNOWLEDGEMENTS

I would like to thank my family, my laboratory collegues (namely, Lucas Costa Campos, Paulo César Pereira and Everton Lima), and especially my advisor Sérgio Apolinário, for supporting me throughout these years.

ABSTRACT

In this M.Sc. dissertation we implement Brownian dynamics to investigate the melting processes of colloidal particles confined isotropically with competing interactions represented by a potential tailored in a repulsive-attractive-repulsive fashion as the inter-particle distance increases. The stable configurations of such system is composed of a large diversity of structures, which includes quasi-crystalline, triangular, square, and mixed orderings, as well as, the presence of ornamental patterns such as fringes and holes, which are located, respectively, at the border and interior of the clusters. Our molecular dynamics simulations demonstrate that during the melting process particles are able to swing between some different micro phases. We also tested the fringes stability which demonstrated to be higher than the one found in compact clusters. Finally, we show that, at the high temperature regime, the system loses its angular ordering while still preserves its radial inter-particle confinement, which, ultimately, causes the proliferation of small sub-clusters.

Keywords: Molecular Dynamics. Competing Interactions. Melting Process. Brownian Dynamics. Colloidal Particles. Micro Phases.

RESUMO

Nesta dissertação de mestrado nós implementamos dinâmica browniana para investigar os processos de derretimento de partículas coloidais confinadas isotropicamente com interações competitivas representada por um potencial ajustado em uma forma repulsiva-atrativa-repulsiva a medida que a distância entre as partículas aumenta. As configurações estáveis desse sistema são compostas de uma grande diversidade de estruturas, que incluem organizações quasicristalinas, triangulares, quadradas, e mistas, além da presença de padrões ornamentais como franjas e buracos, os quais estão localizadas, respectivamente, na borda e no interior dos aglomerados. Nossas simulações de dinâmica molecular demonstram que, durante o processo de derretimento, as partículas conseguem balançar entre diferentes micro fases. Nós também testamos a estabilidade das franjas a qual demonstrou ser maior do que a encontrada em aglomerados compactos. Finalmente, nós mostramos que, no regime de temperaturas altas, o sistema perde sua organização angular enquanto preserva seu confinamento radial entre as partículas, que, ultimamente, causa a proliferação de pequenos sub-aglomerados.

Palavras-chave: Dinâmica Molecular. Interações Competitivas. Processo de Derretimento. Dinâmica Browniana. Partículas Coloidais. Micro Fases.

LIST OF FIGURES

Figure 1 - Dynamical patterns obtained for (a) low attraction and (b) high attraction intensity between colloids. (From [8]) 17

Figure 2 - Schematic representation of (a) hexagonal and (b) square lattices, where a is the distances between vertices and θ is 120° in (a) and 90° in (b) 18

Figure 3 - Graphical representation of patchy colloids: the spherical particles (red) are decorated with extended patches (green), creating a more complex structure. (from [24]) 20

Figure 4 - Illustrative examples of self-assembly processes of patchy colloids 20

Figure 5 - Microscopy image of a 2D colloidal crystal with triangular lattice and isotropic dipole-dipole repulsion between the particles. (From [34]) 25

Figure 6 - Orientational correlation function $G_6(r)$ for different effective temperatures Γ. Blue refers to the crystalline, green to the hexatic, and red to the liquid state. The oscillations reflect the arrangement of the particles in shells around a central particle at $r = 0$ and a is the lattice constant. (From [34]) 26

Figure 7 - Snapshots of the (a) crystal and (b) liquid before and after the melting. The scale of the snapshots can be found in the bottom left. (From [44]) 28

Figure 8 - Translational order parameter (blue) and bond orientational order parameter (black) of superparamagnetic colloidal system as a function of the effective temperature. Sharp decrease in the parameters indicates a solid-liquid phase transition. Statistics were applied over 6000 colloids. (From [44]) 29

Figure 9 - The heterogeneous melting of a 5 layers film. Images are $2D$ slices taken from the middle of the film. The liquid regions look almost identical in different layers.(a) 26.7°C: The solid line near the bottom of the image and the white symbol highlights the places where the lakes will be formed.(b) 27.4°C: Liquid began to nucleate. (c) 27.6°C: the solid line region melted into a liquid strip, and the white region has melted into a liquid lake. (d) 27.8°C: Liquid grows

from lakes and strips of liquid. In equilibrium, the entire crystal melts. Scale bar: $5\mu m$. (From [50]) 31

Figure 10 - Twelve defected structures, where the green colour represents triangular arrangements, red represents square structures, and yellow are other types of structures. (from [52]) 32

Figure 11 - Graphic representation of the repulsive potential of a hard sphere with diameter σ 37

Figure 12 - Graphic representation of the square well potential. The width of the well can be controlled by adjusting λ and its strength with ε 38

Figure 13 - Graphic representation of the Lennard-Jones potential. σ is the hard core radius generated by Pauli repulsion and $-\varepsilon$ is the minimum of the well potential . 38

Figure 14 - Representation of the interaction potential for the parameters $\alpha = 2.9$ and $R = 2.0$ 40

Figure 15 - Initial configuration obtained for systems with $N = 384$ particles, for (a) $R = 2.0$ and $\alpha = 1.00$, (b) $R = 2.0$ and $\alpha = 2.90$, (c) $R = 2.5$ and $\alpha = 1.6$, (d) $R = 2.5$ and $\alpha = 3.1$, (e) $R = 3.0$ and $\alpha = 2.4$, (f) $R = 3.5$ and $\alpha = 3.2$ 47

Figure 16 - Schematic representation of a hypothetical small cluster formed by four particles which are represented by circles and indexed by numbers from 1 to 4, where particles 2, 3 and 4 are neighbors of 1. the angle in the counterclockwise direction between the neighbor k and the next neighbor l is θ_{kl}^1. The angle θ_{42}^1 is the largest one and therefore it is not used in the calculation of ξ_1 49

Figure 17 - Convex hull (a) and Delaunay triangulation (b) of the representative cluster with $N = 384$ particles obtained for $R = 3.0$ and $\alpha = 2.4$ 50

Figure 18 - Schematic representation of the ring used to determine the particles considered in the calculation of $\xi(r)$. Only the particles within the ring (green colored disks) are taken into account for the calculation of $\xi(r)$ 53

Figure 19 - Mean value of ξ as a function of the cluster radial size for temperatures $T^* = 0$ (blue squares), $T^* = 9$ (green stars) and $T^* = 18$ (red triangles) for the cases

(a) $R = 2.0$ and $\alpha = 1.0$, (b) $R = 2.0$ and $\alpha = 2.9$, (c) $R = 2.5$ and $\alpha = 1.6$, (d) $R = 2.5$ and $\alpha = 3.1$, (e) $R = 3.0$ and $\alpha = 2.4$, (f) $R = 3.5$ and $\alpha = 3.2$ 54

Figure 20 - Amplified image of the upper part of the cluster shown in Fig. 15(a) ($R = 2.0$ and $\alpha = 1.0$) for an elevated temperature $T^* = 10.0$. Particles having $\xi < 0.85$ and $\xi \geq 0.85$ are indicated, respectively by green and red disks 55

Figure 21 - Minimum energy configurations for the system with $R = 2.5$, $\alpha = 3.1$, $N = 384$, and temperatures (a) $T^* = 0.0$ and (b) $T^* = 2.25$. The disks' colors indicate the lattice in which the particles belong as shown in the legend 55

Figure 22 - Mean value of the percentages of triangular, mixed and square structures as a function of temperature for the cases (a) $R = 2.0$ and $\alpha = 1.0$, (b) $R = 2.0$ and $\alpha = 2.9$, (c) $R = 2.5$ and $\alpha = 1.6$, (d) $R = 2.5$ and $\alpha = 3.1$, (e) $R = 3.0$ and $\alpha = 2.4$, and (f) $R = 3.5$ and $\alpha = 3.2$ 56

Figure 23 - Representations of the various displacements of particle lines related to the transitions between the phases (a) triangular to mixed, (b) mixed to triangular and square, and (c) square to mixed and triangular 58

Figure 24 - Scheme showing how the quantity ξ was calculated in our Monte Carlo simulations. (a) A central particle is represented by a red colored disk. L represents the greatest distance that a second particle can have from the central one so that both can be considered neighbors. The region delimited by the circle of radius L is called the action section. (b) Representation of a cluster containing one central particle and four other surrounding particles. Note that only the particles of indexes 2, 3 and 4 are within the action section, and therefore, are neighboring of the central particle. The fifth particle is not a neighbor of the central particle and therefore does not contribute to the calculation of ξ. The angles θ_{24}^1 and θ_{34}^1 contributing to the calculation of ξ are also shown 60

Figure 25 - Mean value of the percentage of triangular, mixed and square structures calculated for the particles within the centered circumference of radius $R_{cir} = 5.5$, as a function of the temperature for the cases (a) $R = 2.0$ and $\alpha = 1.0$, (b) $R = 2.0$ and $\alpha = 2.9$, (c) $R = 2.5$ and $\alpha = 1.6$, (d) $R = 2.5$ and $\alpha = 3.1$, (e) $R = 3.0$ and $\alpha = 2.4$, (f) $R = 3.5$ and $\alpha = 3.2$ 63

Figure 26 - Time average of η, defined by the ratio between the areas of the convex hull and altered Delaunay triangulation. The cases $R = 2.0$ with $\alpha = 1.0$ and $R = 2.5$ with $\alpha = 3.1$ (green) represent the compact systems where the ground states are triangular and squared, respectively, whereas the case $R = 3.0$ with $\alpha = 2.4$ represents the systems with fringes appearing in the ground state 65

LIST OF TABLES

Table 1 - Summary of correlations and the Frank constant predictions of the KTNHY theory of two-dimensional melting 26

Table 2 - Set of parameters used to generate the specific structures depicted in Fig. 15 with their correspondents macroscopic properties 51

Table 3 - Average percentage of the number of neighbors for the case of high temperatures ($25.0 \leqslant T \leqslant 30.0$) for all six set of parameters 59

Table 4 - Set of the structures probabilities obtained in the Monte Carlo simulations with random positions for different number of neighbors 61

Table 5 - Monte Carlo simulations percentages of triangular, mixed and square aggregates for the case of high temperatures ($25.0 \leqslant T \leqslant 30.0$) for all six set of parameters 62

Table 6 - Molecular dynamics simulations results of the average and standard deviation of the percentages of triangular, mixed and square aggregates for the case of high temperatures ($25.0 \leqslant T \leqslant 30.0$) for all six set of parameters 62

SUMMARY

1 INTRODUCTION 14
1.1 COLLOIDAL SUSPENSIONS 15
1.2 SELF-ASSEMBLY OF COLLOIDS 16
1.2.1 Collective Behavior 16
1.2.2 Colloidal Synthesis 19
1.2.3 Confined Colloids 20
1.3 TWO-DIMENSIONAL MELTING 21
1.3.1 KTNHY Theory 22
1.3.2 Influence Of An Attractive Interaction On Melting 26
1.3.3 Inhomogeneous Melting 29
1.4 OVERVIEW OF THE CHAPTERS 30
2 MOLECULAR DYNAMICS AND MONTE CARLO SIMULATION 33
2.1 MODELS FOR MOLECULAR DYNAMICS SIMULATIONS 33
2.2 INTERMOLECULAR POTENTIALS 36
2.3 EXTERNAL TRAP 40
2.4 MONTE CARLO METHODS 41
3 SIMULATION ALGORITHM AND STRUCTURES' CLASSIFICATION 44
3.1 LANGEVIN AND BROWNIAN DYNAMICS 44
3.2 POTENTIAL PARAMETERS 45
3.3 SIMULATIONS DETAILS 46
3.3.1 Annealing Method 46
3.3.2 Heating Method 47
3.4 STRUCTURES' CLASSIFICATION 48
3.4.1 Microscopic Structural Ordering 48
3.4.2 Macroscopic Structural Ordering 50
4 MELTING PROCESSES ANALYSIS 52
4.11 PHASE TRANSITION OF THE MICROSCOPIC ORDERING 52
4.1.1 Low Temperature Regime 52
4.1.2 High Temperature Regime 57
4.2 CONFINED MELTING 62

4.3 PHASE TRANSITIONS OF THE MACROSCOPIC ORDERING 64
5 CONCLUSIONS 66
BIBLIOGRAPHY 68

1 INTRODUCTION

This M.Sc. dissertation investigates the melting scenario of two-dimensional ($2D$) confined colloidal particles interacting through a repulsive-attractive-repulsive potential type. We are interested in numerical approaches for evaluation of the microscopic processes undergone by the colloids, i.e., we will not analyze the melting through a thermodynamic viewpoint. We will demonstrate that the system investigated in this work has a melting process significantly different from that found for a system whose interaction potential is purely repulsive.

This chapter starts by introducing the very notion of colloids with some historical background on experiments and simulations as well as their main properties. It follows with briefs discussions on the general theory of two-dimensional melting and its applicability to coloidal systems. The chapter ends with an overview of this dissertation, explaining what information will be found in the following chapters.

Colloidal systems are present in the history since the beginning of life, since they are the essence of formation of many cellular structures, however the field of study of colloidal systems has only been introduced in 1861 by the Scottish scientist Thomas Graham. The techniques Graham used were simple observations of some insoluble particles in water mixtures that did not sedimentate. Initially, these observations were performed with the use of microscopes, however, in the beginning of the 20th century, the experimental methods were enhanced when X-ray diffraction patterns ideas were possible. These patterns are much used in crystallography because atoms of crystals are able to diffract X-ray beams into specific directions depending on the crystal' structure. Today, the most used tool for observation of microscopic colloids is video microscopy, where the frame rate of the video can investigate in real time the dynamics of many systems. The invention of computers also allowed the numerical investigations of colloidal systems that were extremely daunting for humans to perform. Today, computer simulations, with the help of molecular dynamics and Monte Carlo algorithms, are widely used in the literature as they are inexpensive and their processing power grows more potent by the day.

1.1 COLLOIDAL SUSPENSIONS

In chemistry, a colloid is technically a mixture in which one substance of microscopically dispersed insoluble particles (solutes) is suspended throughout another substance (solvent). However, the name colloid is usually referred to the dispersed substance alone and the overall mixture has been generally named by the terms colloidal suspension or colloidal systems. Contradictory to a solution, whose solutes are dissolved in the solvent, forming only one phase, colloidal systems consist of two or more phases, depending on the number of different solutes. Also, to be considered a colloidal suspension, sedimentation must not occur or takes a long time to occur in the mixture.

The dispersed particles usually have a radius, considering they are spherical, between $1nm$ and $1\mu m$, and therefore, the analytical approaches can vary depending on the colloidal system in question. Usually in scientific reports, classical mechanics with some aspects of thermodynamics are used to describe these systems, instead of quantum mechanics.

An important phenomenon that can appear in a colloidal suspension is the formation of colloidal crystals. These are ordered aggregations of colloids that can self-assemble due to the nature of the interaction forces between them. A natural example of this ordering phenomenon can be found in precious opal, in which bright regions of pure spectral color result from dense arrangement of colloidal spheres of silicon dioxide (SiO_2), also known as silica [1]. Opal can be viewed as a colloidal system because the SiO_2 found in it is dispersed throughout other components, such as water and some organic components.

Colloids can also be used as a transport vector of contaminants in water or other liquid surfaces [2]. In biology, life itself can be explained by the transport and aggregate effects of the colloidal substances present in the organism. These substances are called macromolecules, which includes, proteins, carbohydrates, nucleic acids, and they are large molecules composed of a great number of atoms.

In order to numerically simulate colloidal systems, we must first understand the forces that act on the colloids and the consequences of a microscopic particle being suspended on a solvent, that is the drag effect and the Brownian motion. These consequences, as well as the forces acting on the particles, will be explained throughout the chapters. We will also see in the later chapters that colloids can be numerically simulated without the need to microscopically consider the

solvent substances. As Albert Einstein proved in his youth [3], the effects of the solvent over the colloidal particles depends only on the macroscopic parameters, temperature and viscosity, of such solvent.

1.2 SELF-ASSEMBLY OF COLLOIDS

Colloidal systems are widely known for their ability to self-assemble in many types of structures ([4], [5]), being possible to observe microscopic and macroscopic phase transitions. This phenomenon is the result of interacting forces between the particles as well as the external forces acting upon them, therefore the formed structures are highly dependent on the choices of these forces. In this section, we shall describe the main structures formed by colloids.

Self-assembly is defined as the autonomous organization of a system's constituents in complex patterns. Since there is no need for external influence in the self-assembly of colloidal systems, such as crystals, this phenomenon is the main procedure in the fabrication of nanostructured nanomaterials. Even though self-organization methods have been successfully used in the fabrication of new materials ([6], [7]), a better understanding of the dynamics and equilibrium of colloidal systems is imperative, since new complex structures are rising with the passing of time.

1.2.1 Collective Behavior

We start, then, with the revision of some of the most common structures found in the literature. The collective behavior of colloids has been observed in many systems where the interaction potential between the particles consists of an attractive part and a repulsive part. Usually the repulsive part is due to the fact that the colloid has a finite size (generally a sphere), and the molecules that form it repel the molecules of other colloids at short distances. There are many potentials that represent the colloids attractive interactions, but they are mainly represented by a well potential, that is, a potential form in which the well is a region of attraction. More details on the colloid-colloid interactions are given on the next section, for now we will focus on the structures of the colloids only.

A recent example of the collective behavior of colloids can be found in Ref. [8], where H. J.

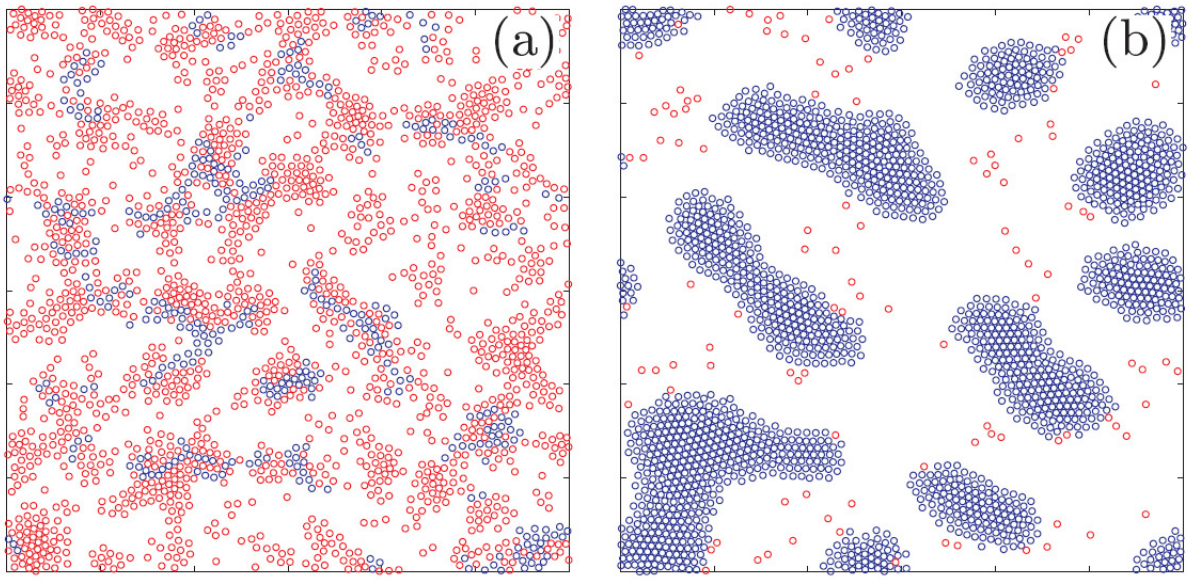

Figure 1 - Dynamical patterns obtained for (a) low attraction and (b) high attraction intensity between colloids. (From [8])

Zhao *et al* numerically investigated the self-organization of colloids with competing interactions (repulsive-attractive interactions) [9]. In Fig. 1 we see the structures observed in their numerical simulations. From Fig. 1(a) to (b) they increased the attraction intensity between the colloids in order to better observe the structures formed by the colloids. We can see that the particles assemble in clusters and these agglomerates in Fig. 1(b) present some geometrical assembly, that is, the particles tend to organize in a triangular arrangement.

These results were obtained with the use of molecular dynamics simulation, which is a standard numerical method widely used for simulating particles, colloids, plasma and many other systems. This method will be described in the next chapter.

Many other works can be found in the literature related to the self-assembly of colloids in various systems, such as biological particles [10], [11], pinned colloids [12], polymers [13] and many others. Futhermore, the geometrical patterns that emerge in these organized structures are of great interest to scientists, since they are the defining factor of macroscopic measured quantities of the system, such as elastic constant, tenacity, and toughness. Many theoretical works have been done in order to determine these physical properties as a function of the microscopic arrangement of the particles. These arrangements do not occur by coincidence, for each one of them has an energy quantity attached, therefore, the system chooses the geometric assembling between particles that minimize this energy.

The most common arrangement found in nature is the triangular arrangement, that is, the

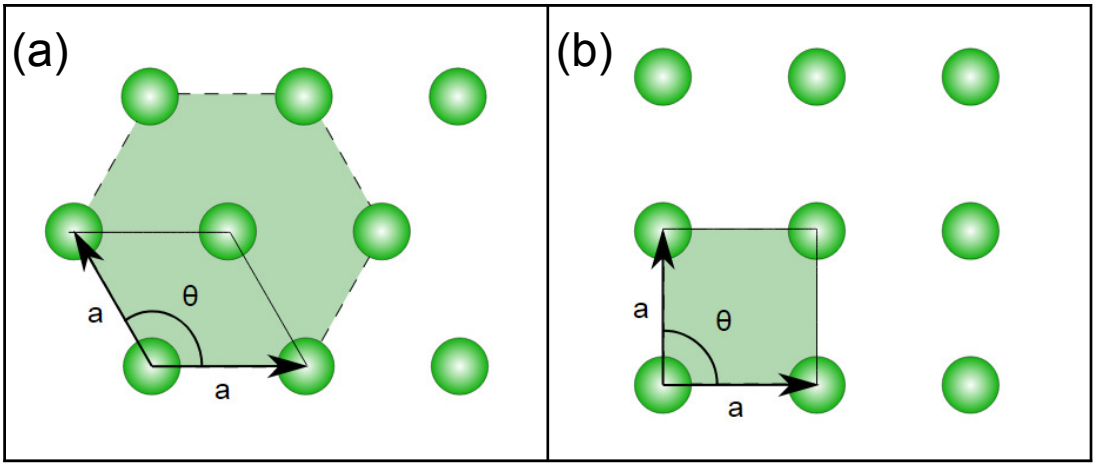

Figure 2 - Schematic representation of (a) hexagonal and (b) square lattices, where a is the distances between vertices and θ is 120° in (a) and 90° in (b).

particles occupy the vertices of a triangular (hexagonal) lattice. Fig. 2(a) shows a representation of a two-dimensional hexagonal lattice, where the distance a can be defined as the lattice constant, since it determines the area of the highlited hexagon. The angle θ in the case of a perfect hexagonal arrangement is, due to geometric symmetry, $\theta = 120°$. In two dimensions, the triangular lattice is the most compact form that disk like particles can arrange, this is the main reason for this lattice to be the most common one found in nature. However, there are many factors that can make the particles assemble in different patterns, for example, in Ref. [14], Zangi and Rice were able to convert the colloids from a triangular lattice to a square lattice, by simply decreasing the density of the system. They concluded in their work that the interaction potential is fundamental for the formation of different geometric patterns. In fig. 2(b) we see a representation of the square lattice, where a serves as the same function as in Fig. 2(a), and θ is simply the normal angle.

The two lattices shown in Fig. 2 are different types of what is called a Bravais lattice. This latter, named after Auguste Bravais, is an infinite set of points in space that localize the vertices of a specific arrangement. Mathematically, a Bravais lattice, in two dimensions, is represented by a generic vector that can localize any point in the lattice. For example, in Fig. 2(a) any vertex can be found by the use of the vector $\vec{R} = n_1\vec{a_1} + n_2\vec{a_2}$, where n_1 and n_2 are integers and $\vec{a_1}$ and $\vec{a_2}$ are represented vectors in Fig. 2(a) with magnitude a. Since a Bravais type of lattice is infinite and periodic in space, it is frequent in analytical studies to calculate the Fourier transform of such lattice. This transformartion is called a reciprocal lattice and it is commonly used in crystalography.

1.2.2 Colloidal Synthesis

To understand the formation of the structures formed in the self-assembly process, we need to understand the interactions between the colloids, and the best way to achieve this is to explain the experimental synthesis of colloids. In this section, we will discuss the influence of the colloid's shape on the interactions form as well as the recent experimental methods used to alter these interactions.

The most common geometrical shape of colloids are usually spherical, which is a simple isotropic shape. There are, however, other shapes created by colloids, such as the rod-like shape which is an anisotropic type. This shape is actually natural to liquid crystals components [15] and it is very important to life (membranes of cells and active component of soap) and technology (screens of devices). Even though the collective behaviour of these rod shaped colloids have been studied over different aspects (see Refs. [16],[17]), their anisotropic aspect makes the mathematical and computational methods quite challenging when compared to spherical colloids. Nevertheless, it is obvious that with more complex colloids we can achieve many different structures with many applications on technology.

With this in mind, in recent years, scientists have been increasing the effort to create more complex colloidal particles with interesting interactions, for now, we are able to patch, chemically or physically, patterned surfaces on the colloids. These colloids are usually called patchy colloids and they can produce different types of anisotropic interactions. These surfaces or, more generally called, patches can be tuned in number, local arrangment, and interaction parameters, allowing many physical phenomena to be investigated, such as the self-assembly of DNA oligonucleotides and proteins [18]-[21]. The usage of patches allowed scientists to induce self-organization processes of systems with nanoscales [22]. In the last decade, it was possible to patch metallic surfaces, like gold and silver, to colloids (see Ref. [23]), allowing applications to eletronic devices. Fig. 3 shows a representation of different patchy colloids where the red spherical particles are decorated with the green patches.

We can see that patches on colloids can be used to create many different interactions between the particles, opening doors to hypothetical interactions models being taken more seriously. It is possible to investigate the self-aseembly of different potentials by the use of computational simulations before the experimental creation of such potentials. Fig. 4 shows illustrative examples of how these patches could work to create a collective behaviour between colloids. The

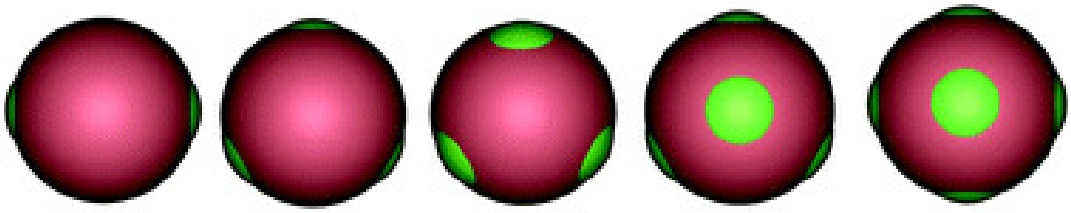

Figure 3 - Graphical representation of patchy colloids: the spherical particles (red) are decorated with extended patches (green), creating a more complex structure.

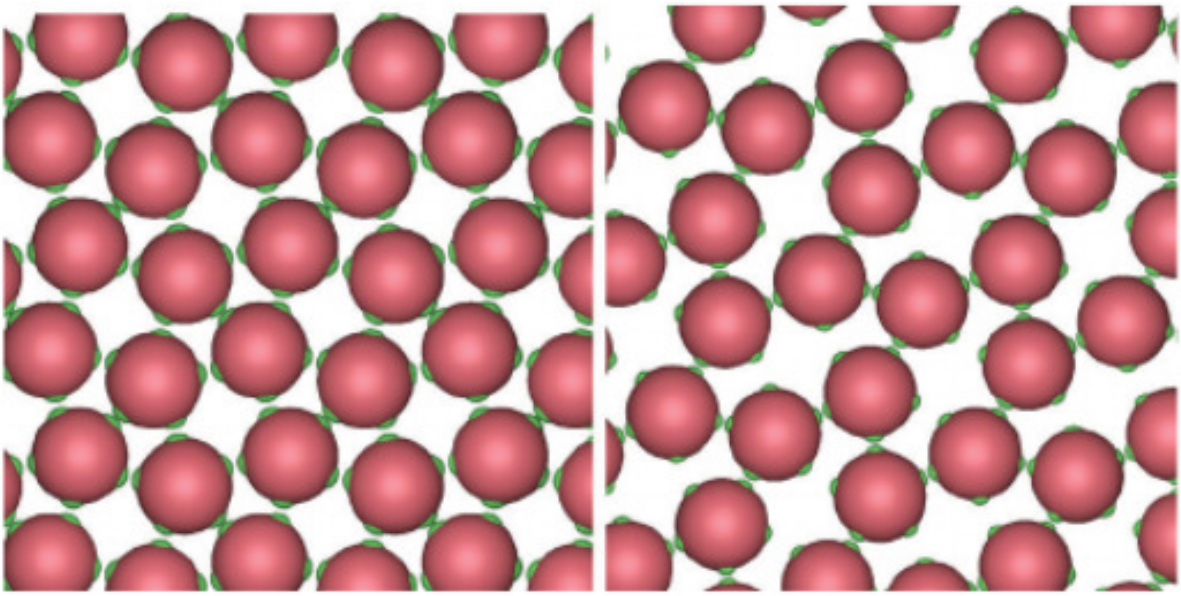

Figure 4 - Illustrative examples of self-assembly processes of patchy colloids. (from [24])

picture was taken from Ref. [24], which is a great review of patchy colloids.

1.2.3 Confined Colloids

Another interesting method to obtain more complex structures is by properly confining the system. In experiments, colloids are usually confined between two walls [25], this is done to better trap the particles in a desired region of interest, such as digital video devices. However, a number of experiments showed that this can actually give rise to interesting structures, such as the ones shown in [26], where it was observed formations of multi-layered lattices of particles between two glass walls. This form of confinement, however, can actually simulate an infinite system if used with a very large number of particles and has very little influence over

the potential energy of them.

A very common confinement is the parabolic trap, which can be experimentally produced by using optical tweezers, where the strongly focused light beams are able to exerce forces on microscopic and even nanoscopic particles, trapping or even driving them in specific regions [27]. This potential is comonly used in dusty plasma systems.

In Ref. [28], Costa Campos et al performed molecular dynamics simulations of parabolic confined colloids interacting through a sophisticated repulsive-attractive-repulsive manner. This interaction potential consisted of a hard disk repulsion merged with a controlled potential well and a Gaussian barrier. Their main interest was to study the system below its crystalline critical temperature. Despite the large number of obtained structures, they were able to identify the preferred particles configurations that minimize the total energy. As expected, due to the large number of particles, these structures were the ground state configurations, since most of the particles accommodate themselves in local energy minima, that is, not global. The structures found presented different types of microscopic ordering, such as triangular and square lattices, as well as an interesting mixed lattice (particle having both triangular and square angles). They also observed different ornamental patterns, such as fringes and holes that perforated the agglomerates.

We were very interested in performing the melting scenario of this system, because to the best of our knowledge, there are not investigations of the melting process for confined systems holding, for instance, a square or mixed ordering. Most of the investigations are for systems where the triangular lattice minimizes the energy.

1.3 TWO-DIMENSIONAL MELTING

In this section, we explain the main properties of two-dimensional melting, since this dissertation focus on the melting processes of the zero temperature crystalline clusters of colloids. We discuss both confined and non-confined systems because depending on the confinement used, the system can still show aspects of infinite systems. We restrict ourselves to two dimensions because the nature of the melting transition in two-dimensional systems seems to be fundamentally different from the transitions observed in three-dimensional systems. This fact has been mainly suggested by Kosterlitz, Thouless, Nelson, Halperin, and Young decades ago, when they published, almost independently, many papers on this topic. The overall theory that emerged

from these works is known today as the KTNHY theory ([29] - [32]) of melting and it is our starting point in understanding the two-dimensional melting process of confined colloids.

1.3.1 KTNHY Theory

The predictions of the KTNHY theory differs strongly from the general first order transition observed in three-dimensional systems. We will explain these main differences with the help of many experiments and simulations that have been done throughout the last years, however, a more detailed explanation of the mathematical approach of the theory can be found in Ref. [29].

If we consider a infinite two-dimensional system with N particles interacting via a repulsive manner in a crystalline state (low temperature T), such as a purely triangular lattice, then the KTNHY theory states that the melting stage of this system consists of a two-step process. The fisrt step is a first or second order transition of the solid phase to a fluid like phase called hexatic phase which will be explained later in this section. The second step is a second order transition from the hexatic phase to the liquid phase. To start explaining this process, we take the system and calculate its positional correlation function. This latter is a quantity that defines the influence that a given particle's translation has on the position of another particle. This positional correlation function is usually given by

$$g_T(|\vec{r}-\vec{r}'|) = \left\langle e^{-i\vec{G}\cdot(\vec{r}-\vec{r}')} \right\rangle, \tag{1}$$

where $\vec{G}$ is the reciprocal lattice vector of the triangular lattice in the colloidal system, and the brackets denote an average over particles at position $\vec{r}$ and $\vec{r}'$. In a three-dimensional solid crystal, this correlation function decays at long distance to a nonzero constant, which means that the translation of a particle always has an influence over another particle's position. This property is defined as long-range order, however an old careful study done by Mermin and Wagner ([33]) shows that long-range order does not occur for the positional correlation function in two-dimensional systems.

At low temperature, a two-dimensional crystal presents what is known as a quasi-long-range translational order. This latter occurs when the positional correlation function (Eq. 1) exhibits a slow power-law decay with exponent η:

$$g_T(|\vec{r}-\vec{r}'|) = g_T(r) \propto r^{-\eta}, \tag{2}$$

where r represents the distance $|\vec{r}-\vec{r}'|$. As the temperature increases, thermal motion of the particles begins to rise and the amplitude of g_T gets smaller, which means that the effects of the translations of particles become less significant at long distances. This connection break between the translation of particles is known as dislocation unbinding. At the melting critical temperature of the crystal (T_m) the exponent η achieves values between $\frac{1}{4} \leq \eta(T_m) \leq \frac{1}{3}$. After the melting transition, that is, when the system is in the liquid phase, the correlation function decays exponentially defining a short-range order, meaning that a particle's movement influences at maximum its first neighbors.

Besides the quasi-long-range positional ordering already described, there is long-range order in the orientation of the nearest neighbors' bonds. We can take the same colloidal system and calculate the correlations between the bond-angles formed by particles in the triangular lattice by following the equations

$$g_6(|\vec{r}-\vec{r}'|) = \left\langle q_6(\vec{r}) q_6(\vec{r}') \right\rangle, \tag{3}$$

$$q_6(\vec{r}_j) = \frac{1}{n} \sum_{k=1}^{n} e^{-6i\theta_{jk}}, \tag{4}$$

where $g_6(|\vec{r}-\vec{r}'|)$ is the bond-orientational correlation function, q_6 measures the orientation of the n neighbors of particle j, and θ_{jk} is the bond angle between particles j and k. With the factor 6, $|q_6|$ can reach a value of one in the perfect triangular lattice, while defects and disorder can reduce the value. In this dissertation we do not use this parameter because it is a good indicator of how close the lattice is to a triangular lattice, however, in our work we explore different arrangements and the interpolation between them. In Chapter 3 we will define the parameter used in our work and further explain the advantages of using it, instead of q_6.

As we have explained, at low temperature, Eq. 3 decays to a nonzero constant, and therefore it is of a long-range order type. However, as the temperature approaches T_m, Halperin and Nelson found that the dislocation of particles, which destroys the quasi-long-range positional order, left a fluid characterized by quasi-long-range order in the nearest neighbors bond-orientations. Therefore, at T_m, g_6 also displays a power-law decay with the form

$$g_6(|\vec{r}-\vec{r}'|) = g_6(r) \propto r^{-\eta_6(T)}, \tag{5}$$

where $\eta_6(T)$ is given by

$$\eta_6(T) = \frac{18 k_B T}{\pi K_a}, \tag{6}$$

where k_B is the Boltzmann constant and K_a is called the Frank constant. K_a is infinite in the solid phase and zero in the liquid phase, however it achieves finite and nonzero values between T_m and a higher critical temperature defined as T_i. At temperatures T_i, K_a discontinuously drops from $K_a = 72/\pi$ to zero, then at temperatures higher than T_i the bond-orientation correlation function decays exponentially, which means that both the orientational and positional order are of short-range type, describing the usual isotropic liquid. This connection break between the bond-angles of particles is known as disclination unbinding.

Therefore, this fluid phase that occurs between T_m and T_i is characteristic of two-dimensional melting and it is called the hexatic phase. It is a fluid where no long-range positional order occurs, but the system still preserves the bond-orientation quasi-long-range order. This means that two-dimensional melting is actually a two-step melting, the first being the transition between the solid and the hexatic phases, and the second being the transition from the hexatic to the liquid phase.

For many years after the proposition of the KTNHY theory many experiments and simulations have been done in order to explore and find the hexatic phase ([34]-[39]). In Ref. [34] Urs Gasser *et al* suspended colloidal particles with a diameter of 4.5 μm in water. The particles were fixed by gravity to the water-air interface of a hanging water droplet. They applied an external magnetic field $\vec{B}$ perpendicular to or slightly tilted by an angle θ relative to the colloid plane. As the particles are super-paramagnetic due to doping with Fe_2O_3 nanoparticles, the field induces a magnetic moment $\vec{M} = \chi B$ in each particle, where χ is the magnetic susceptibility. The resulting dipole-dipole interaction is repulsive and $\propto 1/r^3$ when the field is perpendicular to the colloid plane. They observed the particles by using video microscopy, being able to determine the coordinates of around 2000 particles.

In Fig.5 we see a microscopy image of the 2D suspended colloids with dipole-dipole repulsion arranged in a triangular lattice. They were able to control the system temperature by increasing the strength of $\vec{B}$ and defined the inverse temperature $\Gamma \propto B^2/T$ of the system. Fig. 6 shows the bond-orientation correlation function $G_6(r)$ obtained by them for different temperatures. A transition from long-range to quasi-long-range orientational order is observed at $\Gamma = 48.5$, as for lower Γ values $G_6(r)$ does not approach a constant value at large r but is well described by a power-law expression. They also observed that at the same effective tem-

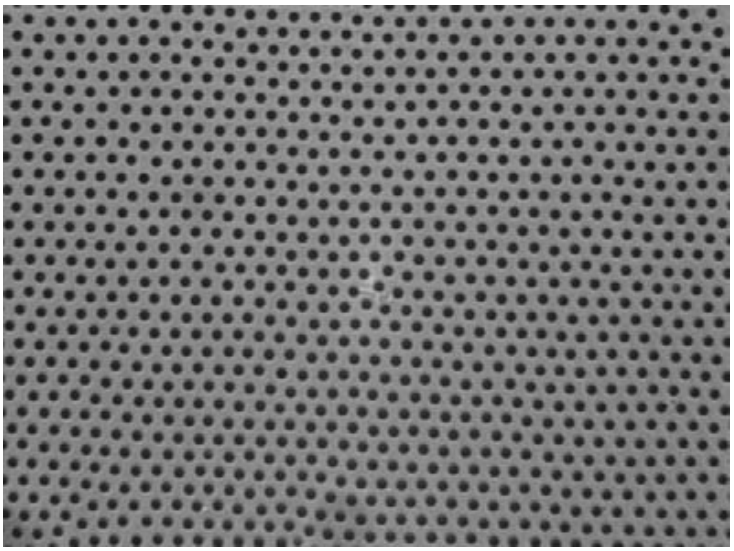

Figure 5 - Microscopy image of a 2D colloidal crystal with triangular lattice and isotropic dipole-dipole repulsion between the particles. (From [34])

perature the translational order changes from quasi-long-range to short-range. We can also note from Fig. 6 that a $G_6(r)$ decays exponentially for higher temperatures, confirming the KTNHY melting scenario.

Other works with dipole-dipole repulsive interactions have been investigated both numerically ([37]), and experimentally ([38]) with the help of video microscopy and they all confirmed the existence of an hexatic phase. Melting simulations using hard spheres as the colloids have also been investigated, for example, in Ref. [36], where Etienne P. Bernard and Werner Krauth used Monte Carlo algorithms to investigate such melting. They confirmed the emergence of the KTNHY scenario as well as the type of transition for each phase. The solid-hexatic transition seems to be of a continuous type, while the hexatic-liquid step is a first order. This latter fact is confirmed by other works (see, for instance, Refs. [35], [39]).

We should note that all of the mentioned investigations of two dimensional melting focused on systems with triangular arrangements. However, there have also been investigations on systems with different symmetries, such as in Ref. [40], where it was studied the melting of a crystal with square symmetry. Curiously, the melting of their system followed a first order transition, not respecting the KTNHY scenario, indicating that the transitions from solid to liquid are sensitive to the type of symmetry observerd in the systems.

In our system we did not observe a stable hexatic phase, however, we believe this to be mainly caused by the attractive part of the interaction potential, as we will explain later. Despite

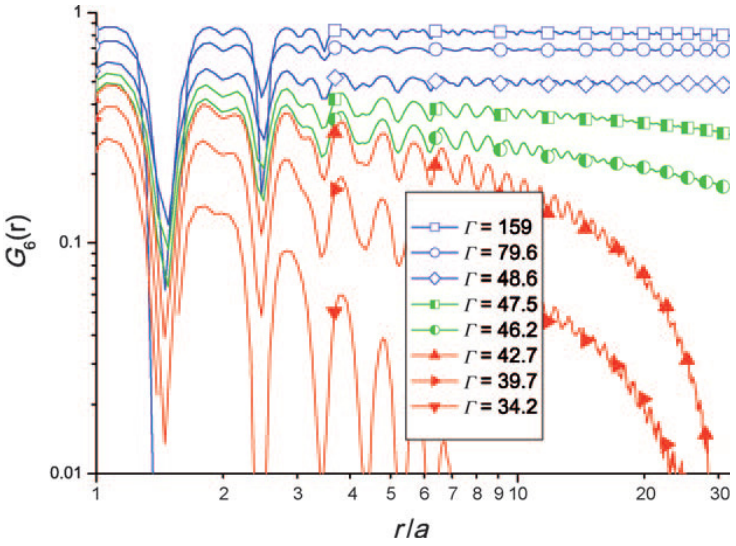

Figure 6 - Orientational correlation function $G_6(r)$ for different effective temperatures Γ. Blue refers to the crystalline, green to the hexatic, and red to the liquid state. The oscillations reflect the arrangement of the particles in shells around a central particle at $r = 0$ and a is the lattice constant. (From [34])

	Solid	**Hexatic**	**Liquid**
Positional Correlation	Quasi-long-range	Short-range	Short-range
Bond-orientation Correlation	Long-range	Quasi-long-range	Short-range
Frank constant K_a	Infinite	Finite, nonzero	Zero

Table 1 - Summary of correlations and the Frank constant predictions of the KTNHY theory of two-dimensional melting.

that, we did observe a change in the microscopic arrangement before the complete melted stage, resembling a two-step melting scenario.

To conclude our discussion on the KTNHY theory we present in Table. 1 a summary of the main properties of the systems for the different phases of two dimensional systems.

1.3.2 Influence Of An Attractive Interaction On Melting

Even though the KTNHY melting scenario has been widely appreciated by scientists due to the interesting two-step melting, it is a phenomenon whose occurrence is very sensitive to the form of the interactions between particles. In systems with purely repulsive interactions, the predictions of the KTNHY model are in good accordance with the experiments and simulations

performed, with a stable hexatic phase found between the solid and liquid phases. However, as we will discuss now, attractive colloid-colloid interactions can tilt the temperature where the hexatic phase occurs or even impede its formation, making the melting a purely first order solid to liquid transition.

As we have already explained, most of the works found in the literature concerning dynamical and equilibrium properties of two-dimensional colloidal systems refer to particles interacting in a repulsive manner. The melting behavior of these systems generally respect the predictions made by the KTNHY theory. However, the sensitivity of such phase was indicated when Blandon and Frenkel (see Ref. [41]) reported in 1995 the results of simulations of a two-dimensional assembly of disks. They interacted via a pair additive potential consisting of a hard core repulsion and a very narrow square well attraction. When the width of the attractive well was less than 8% of the hard disk diameter, the system supported two ordered solid phases with the same packing symmetry but different densities. The solid-solid transition line occurred at a critical point, near which density fluctuations render the solid unstable with respect to dislocation unbinding, and the system supported a hexatic phase. When the square well width was large enough to permit a stable lower density solid phase, the region of stability of the hexatic phase occurred between those of the two solid phases. For the case when the square well width was close to the limiting value for which the lower density solid phase became unstable, the hexatic region was extended to the melting line. Then the sequence of transitions became solid-hexatic-liquid rather than solid-hexatic-solid.

Blandon and Frenkel also noted that the region of stability of the hexatic phase shrinked drastically as the width of the well decreased. They predicted that in the limit that the well width becomes zero or when it is of order 1% of the hard disk diameter, the melting transition is a fisrt order solid-liquid type. These predictions may seem inconclusive, however melting experiments using video microscopy of stabilized uncharged polymethylmethacrylate (PMMA) partciles [42] and suspended uncharged silica spheres [43] proved to be qualitatively consistent with the results of Blandon and Frenkel's simulations.

In more recent work (see Ref. [44]), Di Du *et al* studied the melting of paramagnetic colloids with long-range attractive interactions that resembled the Lennard-Jones Potential. That is, a short-range repulsion and a long-range well potential with depth ε. The attractive interaction between the colloids were induced by the use of a high-frequency rotating magnetic field, which was monitored by using a digital oscilloscope. The dynamics of the colloidal particles

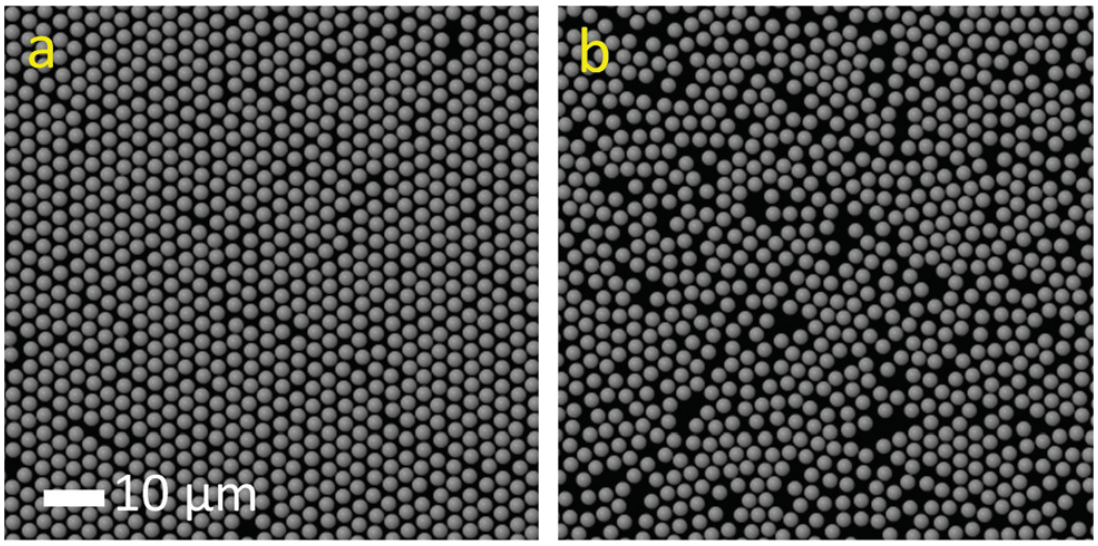

Figure 7 - Snapshots of the (a) crystal and (b) liquid before and after the melting. The scale of the snapshots can be found in the bottom left. (From [44])

were monitored with a CCD camera, which is a device wherein charges can be interacted with light. They observed that the melting is a first order solid-liquid type with no hexatic phase, contradicting the KTNHY scenario.

Figs. 7(a) and (b) show snapshots of the crystal and liquid, respectively, right before and after the transition (the scale of the snapshot is written in the bottom left). In the solid phase the colloids arranged in a triangular lattice, then, with this information the authors of Ref. [44]) defined their translation and orientational order parameters Ψ_T and Ψ_6 in order to determine a critical effective temperature ($T_{eff} = k_B T/\varepsilon$). A sharp decrease in an order parameter indicates the occurrence of a phase transition and Fig. 8 indicates that both Ψ_T and Ψ_6 undergo sharp transitions at $T_{eff} = 0.119$, which indicates that dislocation and disclination unbinding occurs simultaneously, characterizing a first order solid-liquid transition.

Therefore, they could not observe a two-step melting in a system with long range attraction. We can conclude that particle-particle interactions can profoundly influence the character of the melting transition in two-dimensional systems. This latter fact will be evident in our study, since the interaction between the colloids have a significant attractive part.

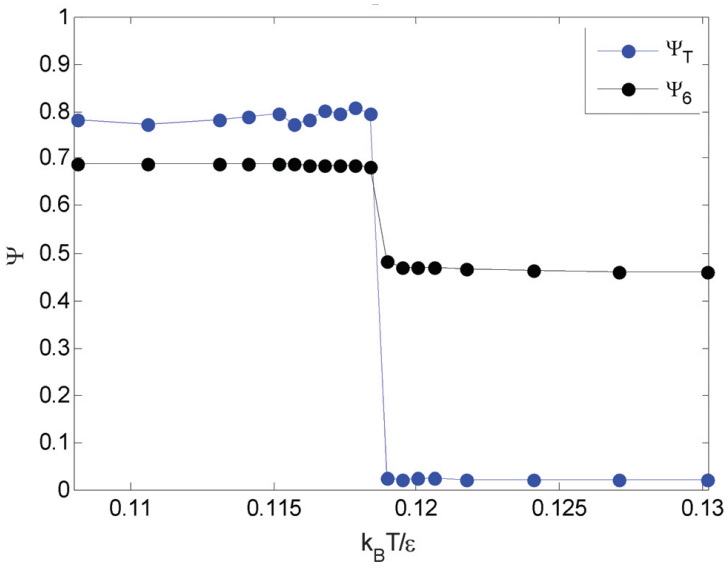

Figure 8 - Translational order parameter (blue) and bond orientational order parameter (black) of superparamagnetic colloidal system as a function of the effective temperature. Sharp decrease in the parameters indicates a solid-liquid phase transition. Statistics were applied over 6000 colloids. (From [44])

1.3.3 Inhomogeneous Melting

Until this point we have described the melting studies of systems that have well-determined critical temperatures, however, there are systems where the definition of a critical temperature is not plausible [45]. In such systems, like confined Coulomb balls [46], we observe what is called a inhomogeneous or heterogeneous melting where, contrary to the homogeneous melting, the dislocation unbinding of the particles does not occur with equal strength in all regions of the system. This means that some regions of the system may be in a crystalline configuration while others are in a liquid state. This type of melting is not investigated as much as the homogeneous type, since thermodynamics cannot be easily applied in these systems. Usually, inhomogeneous melting occurs in systems with confinement that signficantly influences the energy content of the system ([47]-[49]).

To exemplify this, lets look at recent work done by Y. Peng *et al* (see Ref. [50]), which used video microscopy to investigate the melting behavior of multilayered colloidal crystals composed of repulsive micro-gel spheres with diameters close to $1\mu m$ confined between two walls. They were able to control the number of colloidal layers confined between two glass

walls by using different film thickness. it was observed that by using a thin film (1 layer of colloids) the melting process was homogeneous, since this case is the usual two-dimensional infinite system, however thicker films produced inhomogeneous melting. In these multi-layered systems, the colloids gained thermal motion in different regions, forming "lakes" and "strips" of particles surrounded by crystalline structures.

Fig. 9 shows a $2D$ slice of a 5 layers film, where Fig. 9(a) represents the colloids in a crystalline state with triangular arrangement. Fig. 9(b) and (c) shows the inhomogeneous formation of lakes and strips of particles, while Fig. 9(d) indicates that the system eventually converges to a fully melted scenario.

In systems with such heterogeneous melting, it's accetable to analyze the changes of structures over a microscopic point of view [51], that is, to study the defects of the microscopic arrangements. Examples of such defects are given in Fig. 10, where the green, red, and yellow colored structures represents triangular, squared and other arrangements, respectivelly. In our work, we analyze these types of defects with the help of a geometric parameter defined as ξ, which will be explained in Chapter 3. It's worth noticing that these defects are not studied only in heterogeneous melting, for instance, in Ref. [52], the author studies arrangements of defects of a Yukawa system with a well established melting critical temperature.

Therefore, we can conclude that, not only the interaction potential plays an important role in the melting scenario, but the confinement used to trap the colloids can also affect the melting process. In this dissertation we used both a strong confinement that alters the energy of the system and a potential with both attractive and repulsive parts and, therefore, expected to observe a melting scenario with rich information. As we will discuss in the later chapters, we observed that our system did not follow the KTNHY and grain-boundary predictions as the melting process was clearly heterogeneous due to the confinement used. However, it is still inconclusive to us what would be the effect of the potential if the system was not confined.

1.4 OVERVIEW OF THE CHAPTERS

This dissertation is organized as follows. This first chapter serves as an introduction where we have explained the purpose of this work, as well as the most fundamental aspects of colloids, self-assembly and melting. In chapter 2 we will engage a discussion on the concepts of molecular dynamics simulation. The main types of potentials used to model intermolecular

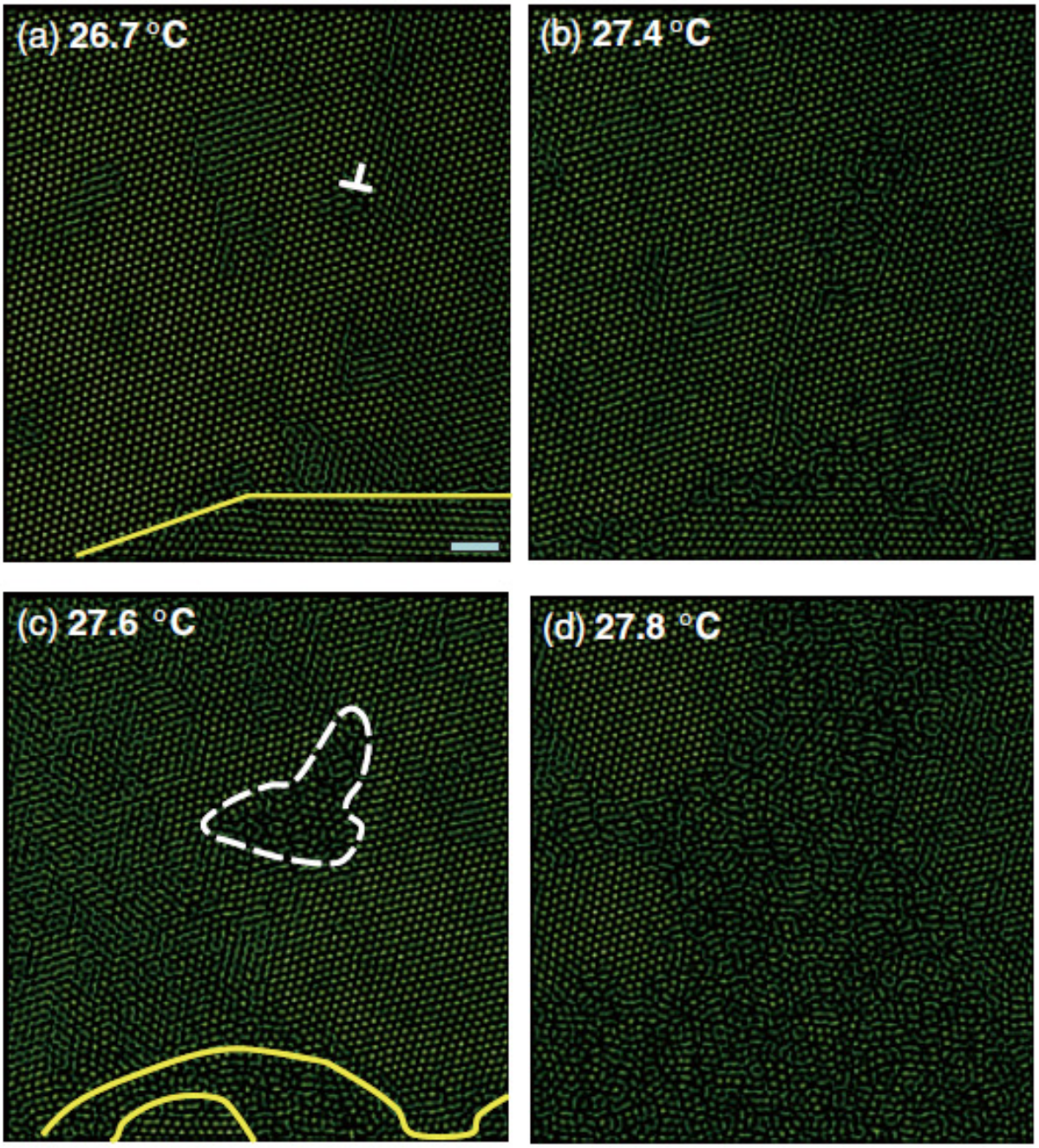

Figure 9 - The heterogeneous melting of a 5 layers film. Images are 2*D* slices taken from the middle of the film. The liquid regions look almost identical in different layers.(a) 26.7°C: The solid line near the bottom of the image and the white symbol highlights the places where the lakes will be formed.(b) 27.4°C: Liquid began to nucleate. (c) 27.6°C: the solid line region melted into a liquid strip, and the white region has melted into a liquid lake. (d) 27.8°C: Liquid grows from lakes and strips of liquid. In equilibrium, the entire crystal melts. Scale bar: $5\mu m$. (From [50])

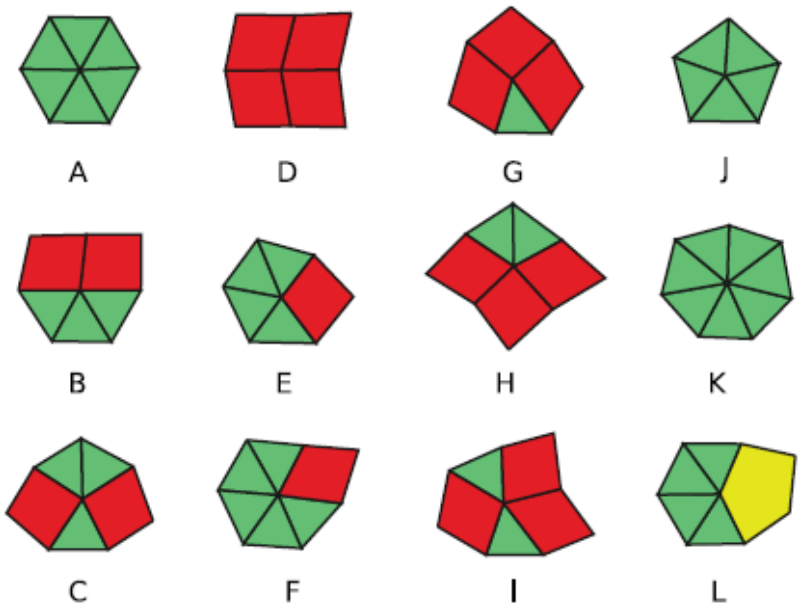

Figure 10 - Twelve defected structures, where the green colour represents triangular arrangements, red represents square structures, and yellow are other types of structures. (from [52])

interactions and confinements are also discussed. In the last part of the chapter we briefly talk about the Monte Carlo method and when it's convenient to use it in many-body systems.

In chapter 3 we investigate the dynamics equations that give rise to the numerical algorithm used in this work. Furthermore, we discuss with more details the initial configurations that will be used in the melting simulations. These were obtained by previous works done by Costa Campos et al [28] where they investigated the static properties of confined colloids with competing pair interactions, in which the potential was of a repulsive-attractive-repulsive type.

Also in chapter 3, we will explain the parameters used to classify, quantify and differentiate of what will be defined as the microscopic and macroscopic structures formed by the particles. These parameters proved to be very useful below the system crystalline critical temperature, as well as at high temperature regime.

In chapter 4 we turn to the analysis of the simulations results of the melting scenario. We divide the chapter in order to clarify the different aspects of the melting process, that is, we investigate the thermal effects both at low and high temperatures, we explain the effect that the external potential has on the melting scenario, and we also study the stability of macroscopic patterns in the end of the chapter. We will, throughout the chapter, explain the methods used to analyze the simulations data, since they are specific to our system. Our final conclusions of this dissertation are given in chapter 5.

2 MOLECULAR DYNAMICS AND MONTE CARLO SIMULATION

The ability to peform numerical simulations with the use of computers have forever changed the field of many-body systems. The computation of the equations found in these systems is a extremely daunting task for humans, since the coupling between equations become more complicated as the number of components increase. However, as time passes, computer processors grow more potent, allowing, with the use of numerical algorithms, the iterations of such equations to be performed in an appreciable time. The most used algorithms in many particles systems are the molecular dynamics and the Monte Carlo methods. These have been widely used to simulate colloidal particles [53], complex plasmas [54], and even biological systems such as the formation of lipid membranes [55].

We will start this chapter by making a brief discussion about the essence of Molecular Dynamics simulations and the systems that are normally studied by means of this method. We then explain models of intermolecular potentials that gives shape to the particles, such as the hard core, the well, and the Lennard-Jones [56] potentials. We shall see that the choice of which potential to use determines which type of problem will be treated in the simulation. Next, we explain typical external traps used for confinement of particles and how can these traps be produced in laboratory. We end the chapter by explaining the Monte Carlo simulation method and when it's convenient to use it.

2.1 MODELS FOR MOLECULAR DYNAMICS SIMULATIONS

Molecular dynamics simulation is a powerful technique used to solve problems of many-body systems for studies related to microscopic phenomena. Given the fact that solving such problems numerically, in a good level of details, without the use of computers is not feasible, molecular dynamics methods have proven to be indispensable.

The model for these methods can be divided in three parts, where the first one accounts for the interactions between the components of the system (particles, colloids, etc) and the second one treats the interaction between these components and the system's boundaries. This can only be done if the intermolecular interactions is independent of the component interactions with the system's boundaries, but this is true for the systems described in this work. The third part is

related to the equation of motion that will be solved to find the trajectories.

For the first part of the model, the interactions between the components is usually represented by an intermolecular potential energy, that gives rise to the forces between them. This potential naturally defines the geometric shape of the individual molecules, this means that by defining the interaction potential we automatically establish the symmetry of the molecules, i.e., if they are rigid or soft, if they are spherical or rod-like. The intensity of the potential will also determines the time passed between iterations, therefore the intermolecular potential must be established before proceeding with any simulation.

In this work, our components will be colloidal particles with spherical symmetry. For a system with N particles, the potential energy of the system is represented by $U(\vec{r}^N)$, where $\vec{r}^N$ represents the set of vectors that localize the centers of mass of the particles, $\vec{r}^N = \vec{r}_1, ...\vec{r}_N$. When we establish a set of values for $\vec{r}^N$, we define a system configuration. The potential energy of the system, $U(\vec{r}^N)$, in the absence of an external potential, is given by the sum of the pairwise interaction and has the form:

$$U(\vec{r}^N) = \sum_{i=1}^{N-1} \sum_{j>i}^{N} u(r_{ij}), \tag{7}$$

where $u(r_{ij})$ is the established intermolecular potential energy between particles i and j, with r_{ij} being the distance between their centers of mass.

In the abscence of dissipative forces, the intermolecular forces are conservatives. Therefore, the force acting on particle i, $\vec{F}_i$, can be obtained by use of the following calculus:

$$\vec{F}_i = -\nabla_{\vec{r}_i} U(\vec{r}^N), \tag{8}$$

where $\nabla_{\vec{r}_i}$ represents the gradient with respect to the position $\vec{r}_i$.

The second part of the model refers to the interaction between the particles and the system's boundaries. The characteristics of these boundaries are mostly determined by the physical situation to be simulated. If we want to simulate an infinite system, we should use a contour condition, for example, we could define a box where the N particles must be located and if a particle would pass one end of the box, it would be transported to the other end, respecting the distance that should be traveled by the particle. For the simulation of a finite system, which is the case of this work, we should use external traps to confine the particles in a region of interest, where these traps can be simulated by the use of external potentials that act upon each particle.

By defining this potential we can immerse it in the total potential energy of the system, $U(\vec{r}^N)$, generalizing Eq. 7 to

$$U(\vec{r}^N) = \sum_{i=1}^{N} V(\vec{r}_i) + \sum_{i=1}^{N-1} \sum_{j>i}^{N} u(r_{ij}), \tag{9}$$

where $V(\vec{r}_i)$ is the external potential acting upon particle i at position $\vec{r}_i$. Defining a conservative external potential is preferable since, by doing so, Eq. 8 would not change.

With the intermolecular and external potentials defined, we can formulate the third part of the model, that is, how the particles will move over time. In the most common version of molecular dynamics, the trajectories of the particles are determined by solving Newton's second law of motion numerically. In this sense, the method is simply the numerical procedure to solve the old idea in science that knowing the initial conditions of the system and all the forces acting on the bodies is enough to calculate the behavior of the system. Therefore, in this version of molecular dynamics, the positions $\vec{r}^N$ can be calculated by solving numerically the following equation:

$$m_i \ddot{\vec{r}}_i(t) = -\nabla_{\vec{r}_i} U(\vec{r}^N), \tag{10}$$

where m_i is the mass of particle i, the dots over $\vec{r}_i$ represents time derivatives, and ∇ is the gradient operator. However, this version of molecular dynamics is not the best to use when investigating colloidal particles, because they are generally suspended in a solvent, which means that the particles interact with the components of the solvent and create the well known Brownian motion. Also the effects of temperature over motion is also significant in these microscopic systems such as colloids, consequently, the right-hand of Eq. 10 has to be generalized to implement these microscopic aspects. The equation of motion that it is commonly used in this situation is obtained from the so called Langevin dynamics and will be explained in Chapter 3.

In short, the method of molecular dynamics consists of two tasks, the first one being the development of the model, which includes the choice of the intermolecular potential, the system's boundaries and the equations of motion. The second task is to numerically solve the equations and produce the trajectories of the particles, in order to analyze them and obtain the statistical and dynamical properties of the system.

2.2 INTERMOLECULAR POTENTIALS

As a first step, before proceeding with a simulation, we must define a function form for the intermolecular potential. In almost every case of many particles systems, the potential energy can be written as a sum, like Eq. 7, where the total energy of interaction between the N particles is the sum of the contributions of pairs of particles. In this section, we will discuss the most important aspects of intermolecular potentials that are relevant to this work.

There are two major types of bodies in molecular dynamics algorithms: soft and hard bodies. Soft bodies are those where the intermolecular potential is continuous with the distance between particles, for example, in confined Yukawa systems [58] the potential consists of an exponential increase with the decreasing of distance. This produces spheres with no defined radius, as they can get as much closer as we want by simply increasing the intensity of the confinement. Hard bodies are those where the intermolecular potential is discontinuous with the distance between particles and as the name implies, they have a well defined radius. The most simple potential for a hard sphere with diameter σ is given by

$$U(r_{ij}) = \begin{cases} \infty & r_{ij} \leq \sigma \\ 0 & r_{ij} > \sigma \end{cases} . \tag{11}$$

The graph for Eq. 11 can be seen in Fig. 11. This type of potential is called hard core potential and it makes the particles interact only during collisions and has the utility to prevent the overlapping of particles. It is worth noticing that these collisions are elastic and therefore conserve the momentum and the total potential energy.

We can modify the hard core potential in order to simulate rigid spheres that, at mid-range or long-range distances, interact through an attractive form. The most simple way to do so it is to add a square well potential to Eq. 11 in the following way:

$$U(r_{ij}) = \begin{cases} \infty & r_{ij} \leq \sigma \\ -\varepsilon & \sigma < r_{ij} < \lambda\sigma \\ 0 & r_{ij} \geq \lambda\sigma \end{cases} , \tag{12}$$

where λ and ε are constants and defines the width and depth of the well, respectively. Fig. 12 shows the graphic representation of Eq. 12 and it shows that the potential well is formed by a short-range hard core repulsion interaction and a mid-range or long-range, depending on λ,

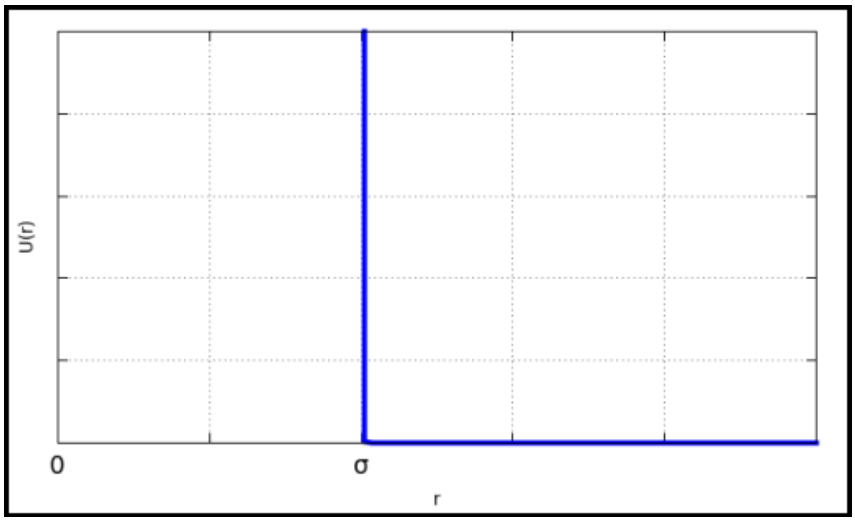

Figure 11 - Graphic representation of the repulsive potential of a hard sphere with diameter σ.

attraction with intensity ε. This potential, even though it is very simple, has enough parameters to produce phase transitions in some systems, for example, we could take N particles with radius R in a infinite system (periodic boundaries) and initiate them in a crystalline state, by increasing the systems temperature over time, we will be able to determine a melting critical temperature.

This repulsion-attraction type of potential is extremely common in nature, especially in molecular systems. In 1924, John Lennard-Jones proposed the most popular attractive-repulsive potential in science, the Lennard-Jones potential. This potential also has two parts, a repulsive part at short ranges, caused by the Pauli repulsion due to the overlapping of electron orbitals, and a attractive part which is commonly named as the Van de Waals or dipole-dipole force. This latter was known to scale with $(1/r)^6$, and using logic, but arbitrarily, the repulsion part was made to scale with $(1/r)^{12}$, which, ultimately, led to the following form:

$$V_{LJ}(r_{ij}) = 4\varepsilon \left[\left(\frac{\sigma}{r_{ij}} \right)^{12} - \left(\frac{\sigma}{r_{ij}} \right)^{6} \right], \tag{13}$$

where $-\varepsilon$ is the minimum of the potential. Fig. 13 shows the graphic form of Eq. 13 and the first thing to note is that the function is continuous, but it captures the hard core aspect due to the potency in the repulsion part. The Lennard-Jones potential is especially accurate for noble gases, with no surprises, since Lennard-Jones modeled this potential while researching liquid argon. In modern times, this potential has been modified in many ways, the most common of them was the generalization of the exponents in Eq. 13 for greater values.

To end this section, we shall describe the potential used in this work. The inter-particle interaction potential is the combination of three parts and is given by

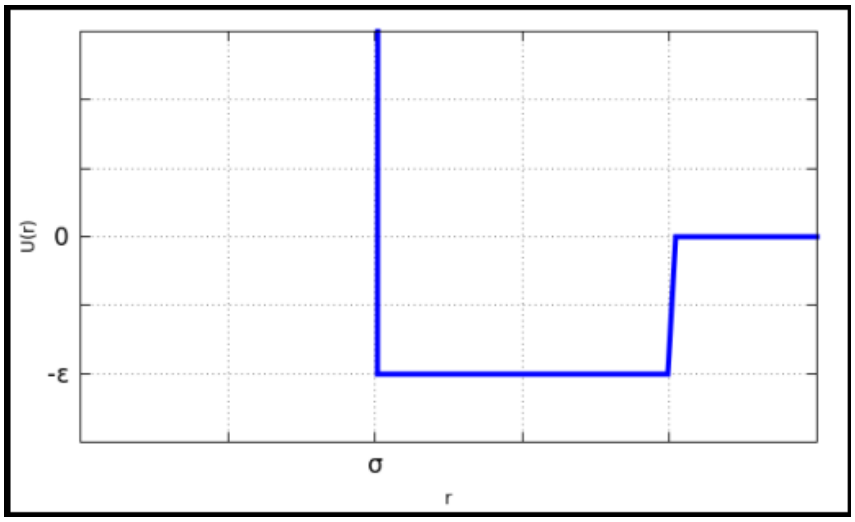

Figure 12 - Graphic representation of the square well potential. The width of the well can be controlled by adjusting λ and its strength with ε.

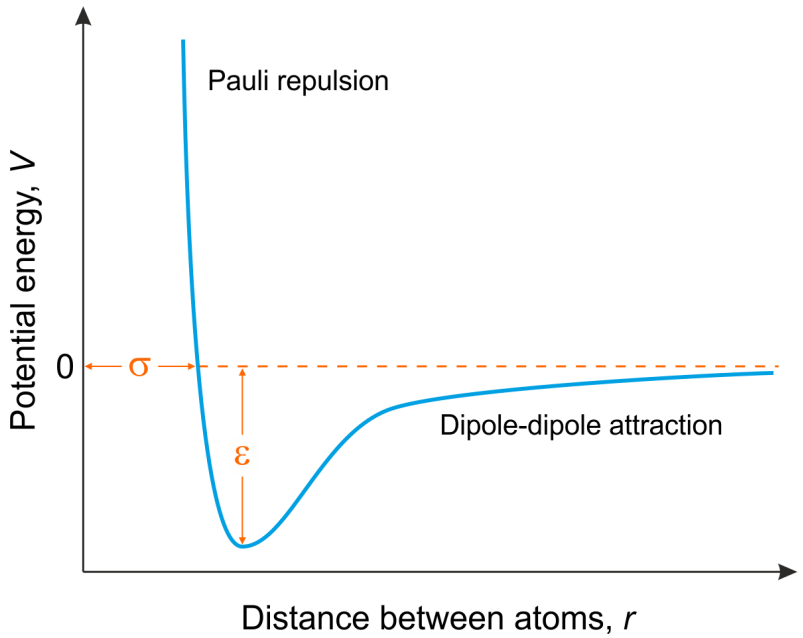

Figure 13 - Graphic representation of the Lennard-Jones potential. σ is the hard core radius generated by Pauli repulsion and $-\varepsilon$ is the minimum of the well potential.

$$U(r_{ij}) = U^{HC}(r_{ij}) + U^{PW}(r_{ij}) + U^{G}(r_{ij}), \tag{14}$$

where $U^{HC}(r_{ij})$ is a short-range hard core repulsive potential, $U^{PW}(r_{ij})$ is a mid-range potential well, and $U^{G}(r_{ij})$ is a shifted Gaussian shaped potential acting on larger distances. This potential is actually quite complex, therefore we shall describe each term separately. Starting with the hard core term, we have its explicit form given by:

$$U^{HC}(r_{ij}) = \varepsilon \left(\frac{2r_o}{r_{ij}} \right)^m, \tag{15}$$

where $2r_o$ defines the diameter of the colloids, m is an exponent which defines how fast the repulsive part increases, which means that if m was infinite this term would simulate a perfect hard sphere. ε gives the strength of the potential, that is, it simulates how susceptible the particles are to it. This term simply defines a radius to the colloids and prevents them from overlapping with each other. The second part, the attractive one, is given below:

$$U^{PW}(r_{ij}) = -\varepsilon \exp\left[-\left(\frac{r_{ij}/r_o - 2}{\alpha} \right)^n \right], \tag{16}$$

This is a more complex potential well, where the exponent n specifies how fast the borders of the well decrease, that is, if n was infinite, then the well would be a perfect quadratic type. The parameter α is a very important one which defines the thickness of the well, which means it can be seen as the radius of imprisonment by the colloid. A very large α means that a colloid can attract very distant particles. This term is quite versatile and it is essential to the formation of complex structures different from the regular compact triangular lattice. The last term, that is, the Gaussian barrier, has the following explicit form

$$U^{G}(r_{ij}) = R\varepsilon \exp\left[-\left(r_{ij}/r_o - \beta \right)^2 \right], \tag{17}$$

where β simply shifts the position of the barrier and R can change its height, that is, it defines the minimumn energy that colloids must have to enter the well region of another colloid. This term was introduced in the potential due to the external trap that we used in the system in order to prevent the trap from destroying interesting configurations. A more detailed explanation of this last fact is given in the next chapter.

In this work we use the value $\beta = 1.5(2+\alpha)$ in order to avoid superposition between the terms $U^{PW}(r_{ij})$ and $U^{G}(r_{ij})$. Fig. 14 shows a graphic representation of the inter-particle interaction potential given by Eq. 14 for the particular situation of $\alpha = 2.9$ and $R = 2.0$. Even though

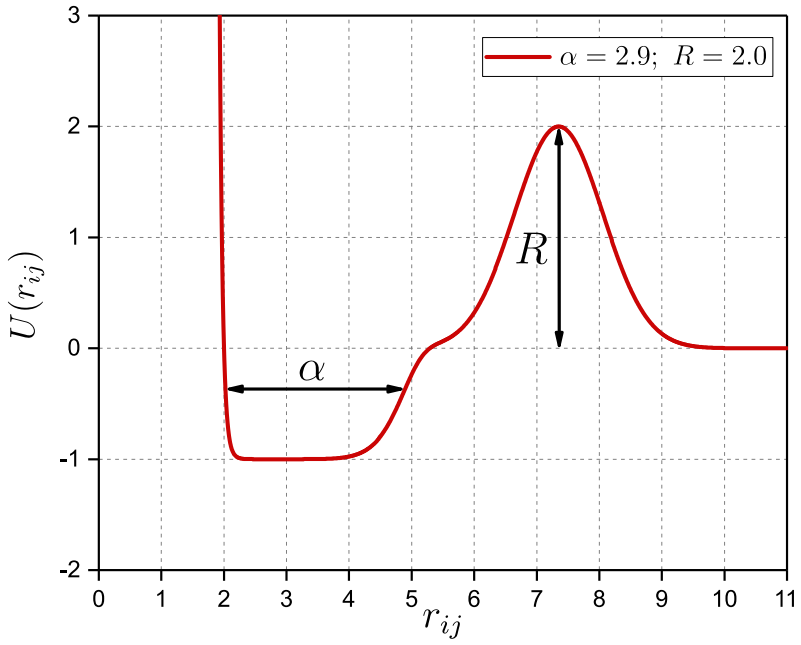

Figure 14 - Representation of the interaction potential for the parameters $\alpha = 2.9$ and $R = 2.0$.

we do not know of experimental investigations of this potential, we expect that the methods of agreggating patches to the colloids surfaces, described in the first chapter, could be used to create experimentally this potential.

This potential has proven to produce a very rich diversity of ground-state configurations for confined colloids [28]. However, if the particles were not to be confined, the interaction potential used in this work, could be simplified to the potential treated in Ref. [59]. In this reference, the interaction potential is given solely by the sum of the two first terms $U^{HC}(r_{ij})$ and $U^{PW\cdot}(r_{ij})$. This means that the Gaussian term $U^{G}(r_{ij})$ is crucial to the formation of a wide variety of structures in the self-assembly process of trapped colloids, in other words, without the Gaussian term, the trapping force would cause the particles to organize only into triangular structures.

2.3 EXTERNAL TRAP

In this section, we shall describe the most common external potentials used to confine and control disperse colloids. These potentials will act upon individual particles, and will be functions of the positions of theses particles. However, it is possible to create external traps that affects the interaction between the particles such as magnetic fields and alternating currents.

In the most simple way, the confinement is treated as rigid walls with zero influence inside the container. If the dimensions of the walls are much bigger than that of the particles, then boundaries' effects can be neglected and thermodynamics can be easily applied, for the system will behave very much like an infinite system. This confinement can be represented by a potential function, with dependence only on the position of the particles, and is given by

$$V_{ext}(r_i) = \begin{cases} 0 & r_i \leq L \\ \infty & otherwise \end{cases}, \tag{18}$$

where r_i is the distance of particle i from the origin, and the walls have a circular form with radius L. Therefore, this potential has the purpose to confine the particles in a region, without affecting their energy.

The external potential that will be used in this work is called a parabolic potential, which is also used to confine plasmas [60], and it is given by the equation

$$V_{ext}(r_i) = \frac{1}{2} V_o {r_i}^2, \tag{19}$$

where V_o is the strength of the potential. The parabolic form of the potential can change the energetic balance of the particles, for they will always feel a force dragging them towards the origin and, as we will see in chapter 4, it affects the melting scenario of colloids interacting through Eq. 14 in a very significant way. This parabolic form of the potential can be experimentally produced with the use of optical tweezers capable of trapping atoms and molecules with focused light beams [61], [62].

2.4 MONTE CARLO METHODS

In this section, we will make a brief discussion on Monte Carlo methods, focusing only on the aspects which are relevant to this work. A more detailed explanation about Monte Carlo simulations can be found in Ref. [63].

Monte Carlo methods are a broad class of computational algorithms that rely on repeated random sampling to obtain numerical results. Their essential idea is using randomness to solve problems that might be deterministic in principle. The methods can be used to solve such a large set of systems that we could write an entire dissertation about them and would still be

missing many systems to refer. Therefore, we will focus on some of the physical systems that Monte Carlo can solve.

In computational and chemical physics, Monte Carlo methods are of extreme importance. They can be used to solve the many-body problem for statistical and quantum systems, in radiation materials science, the binary collision approximation for simulating ion implantation is usually based on a Monte Carlo approach to select the next colliding atom. In astrophysics, they are used in such diverse manners as to model both galaxy evolution and microwave radiation transmission through a rough planetary surface. They are also used in the ensemble models that form the basis of modern weather forecasting. In all these systems, the essence of the Monte Carlo methods are the same, which is, if we know all the accessible states of the system, we can repeatedly sample them by following some deterministic or probability laws, in order to obtain accurate distributions of the states.

To exemplify this, we will use the system investigated in this work, that is, colloidal particles. First, the position of all colloids in a given time would define the systems' state. In the following time step, each of the accessible states has a probability of being accessed which depends strongly on the energy that the system would gain or lose by accessing this state and the temperature of the system. The probability of such states transition can be written as a Boltzmann distribution:

$$P_{transition} = A \exp\left(-\frac{\Delta E}{k_B T}\right), \tag{20}$$

where A is a normalizing constant, ΔE is the energy difference between the states, k_B is the Boltzmann constant, and T is the temperature of the system. Eq. 20 suggests that, if ΔE is negative, that is, the system loses energy, then the new state has a high probability of being accessed. If, however, the opposite were to happen, then the new state would have a very small chance of being accessed. So we could, for example, use the Monte Carlo method in the following way: first define the initial state of the system, second, randomly select another state, then calculate ΔE between them, finally apply the transition law defined for the ΔE type (negative or positive). By repeating this procedure a large number of times we can obtain the state distribution of the system for a given temperature.

Eq.20 also suggests that at high temperature regime, all transition probabilities would be very small and therefore equiprobable. In this case, all the states are equally likely to be accessed. This situation will be very useful in this work, when we analyze the melting process of

the colloidal systems at high temperatures in chapter 4.

3 SIMULATION ALGORITHM AND STRUCTURES' CLASSIFICATION

We will start this chapter by describing the chosen equations of motion of the particles used throughout the simulation. We will also explain how to transform these equations into an simulation algorithm with the help of Brownian dynamics technique [11], which will result in a first-order algorithm obtained from the Langevin dynamics. We then follow with simulational details, such as the time scale of the simulations, the intensity of the potentials, and the method to change the system temperature throughout the simulations.

After the simulations are done, we have to analyze the results by using methods convenient to the system. Therefore, we explain in the last section of this chapter the parameters of classification used to describe the microscopic and macroscopic structures of the system. More information about these parameters can be found in Refs. [28], [59], and [64].

3.1 LANGEVIN AND BROWNIAN DYNAMICS

As we have explained in the last chapter, colloids are generally suspended in solvents (usually fluids). The particles in this solvent have much smaller dimensions than those of the colloids and therefore are extremely numerous in comparison with the colloids, and moreover, these small particles are in constant collisions with the colloidal particles. The effect of these collisions on the dynamics of the colloids is a random movement of particles called the Brownian motion and was one of the first big problems that Albert Einstein studied [3]. In fact, he was able to prove that these random forces that cause the Brownian motion would also cause drag if the particles were pulled through the fluid. This latter fact is called the flutuation-disspitation theorem, which makes the Brownian motion not to depend on the atomic details of the solvent. The two properties of the environment that are relevant to this motion is the viscosity of the solvent, which can be determined by use of hydrodynamics, and the temperature of the system.

It is necessary, then, to formulate an equation of motion that accounts for this random movement of the colloids. The Langevin dynamics is a good candidate, for it not only takes consideration of these effects that but it also allows us to control the temperature as a strength of this random motion. It also simulates the viscous aspect of the solvent, which means that the energy of the particles is no longer conservative. The equation of motion for this dynamics for a

particle at position $\vec{r}_i$ immersed in a solvent with viscosity γ is given by

$$m\ddot{\vec{r}}_i(t) = -\nabla_{\vec{r}_i} U(\vec{r}^N) - \gamma m\dot{\vec{r}}_i(t) + \vec{g}(t)\sqrt{2m\gamma k_B T}, \tag{21}$$

where $U(\vec{r}^N)$ is the total potential acting over particle i and therefore $-\nabla U(\vec{r}^N)$ is the force acting on the particle due to the external and interaction potentials. The dots over $\vec{r}_i$ are used to denote time derivatives, which means that $\dot{\vec{r}}_i$ and $\ddot{\vec{r}}_i$ are the velocity and acceleration of the particle, respectively. T is the temperature of the system, k_B is the Boltzmann constant, and the term $\gamma m\dot{\vec{r}}_i(t)$ is related to the friction of the environment over the particle. $\vec{g}(t)$ is a vector with random direction and with modulus obeying a normal distribution, which means it serves as the random forces caused by the influence of the solvent over the colloids.

As our objective is to use the temperature as a controlling parameter, then we will set a constant viscosity. To find an algorithm to numerically solve Eq. 21 we will investigate the Langevin dynamics in the over-damped case, that is, when there is no average acceleration ($\ddot{\vec{r}} = 0$). This limit is commonly called Brownian dynamics, because it is much easier to analyze the diffusion processes of the Brownian motion in this limit. By normalizing m to 1 (all colloids have the same mass) and setting this limit in Eq. 21 we get

$$\dot{\vec{r}}_i = -\frac{\nabla_{\vec{r}_i} U(\vec{r}^N)}{\gamma} + \vec{g}(t)\sqrt{\frac{2k_B T}{\gamma}}. \tag{22}$$

This equation can be integrated by the use of Euler's method [65], and therefore resulting in the following first order algorithm

$$\vec{r}_i(t+\Delta t) = \vec{r}_i(t) + \frac{\vec{F}_i(t)\Delta t}{\gamma} + \vec{g}\sqrt{\frac{2k_B T\Delta t}{\gamma}}, \tag{23}$$

where $\vec{F}_i(t) = -\nabla U(\vec{r}^N)$ is the force acting on particle i at instant t and Δt is the finite time step used to iterate the equation.

3.2 POTENTIAL PARAMETERS

In this section we make a brief discussion of the inter-particle and external potentials parameters, which are given bellow.

$$U(r_{ij}) = \varepsilon \left(\frac{D}{r_{ij}}\right)^{m} - \varepsilon \exp\left[-\left(\frac{r_{ij}-D}{\alpha}\right)^{n}\right] + R\varepsilon \exp\left[-\left(\frac{r_{ij}-\beta}{0.5D}\right)^{2}\right], \tag{24}$$

$$V_{ext}(r_i) = \frac{1}{2} V_o {r_i}^2. \tag{25}$$

In the external potential we adjust the strength to $V_o = 0.2\varepsilon$ and fix that value throughout the simulations. The most important parameters in the interaction potential is the height of the Gaussian barrier, R, and the thickness of the potential well, α, for these parameters are responsible for the emergence of various complex structures formed by the colloids [64]. The other parameters of the potential are kept constant, that is, $m = 40$, $n = 10$, $\varepsilon = 1$. β is adjusted to $1.5(D+\alpha)$ in order to avoid superposition between the potential well and the Gaussian barrier.

3.3 SIMULATIONS DETAILS

3.3.1 Annealing Method

Before proceeding with the melting, we must first obtain the initial configurations. To do so, we perform molecular dynamics simulations to obtain the ground state structures of the system with a potential ruled by Eq. 24. We have performed simulations similar to the ones done in [28] with 384 colloidal particles with unitary radius. We started the simulation with a random distribution of the particles at temperature $T = 5\varepsilon/k_B$ and followed the annealing method, that is, we thermalize the system at high temperature and then, we slowly decreased the temperature to zero. We have done this for various values of R and α.

We then chose the representative configurations shown in Fig. 15 to use in the melting simulation. These structures represent the ground state configurations of the system and they presented two types of orderings, that is, microscopic and macroscopic orderings. Fig. 15(a) shows a configuration in which the microscopic ordering consists of a triangular lattice, while Figs. 15(b) and (d), show that particles are able to form, respectively, mixed and squared lattices. The macroscopic order refers, for instance, to the presence of fringes that appear at the outer border of the cluster or holes perforating the cluster's center, which can be seen, respectively, in Figs. 15(e) and (f).

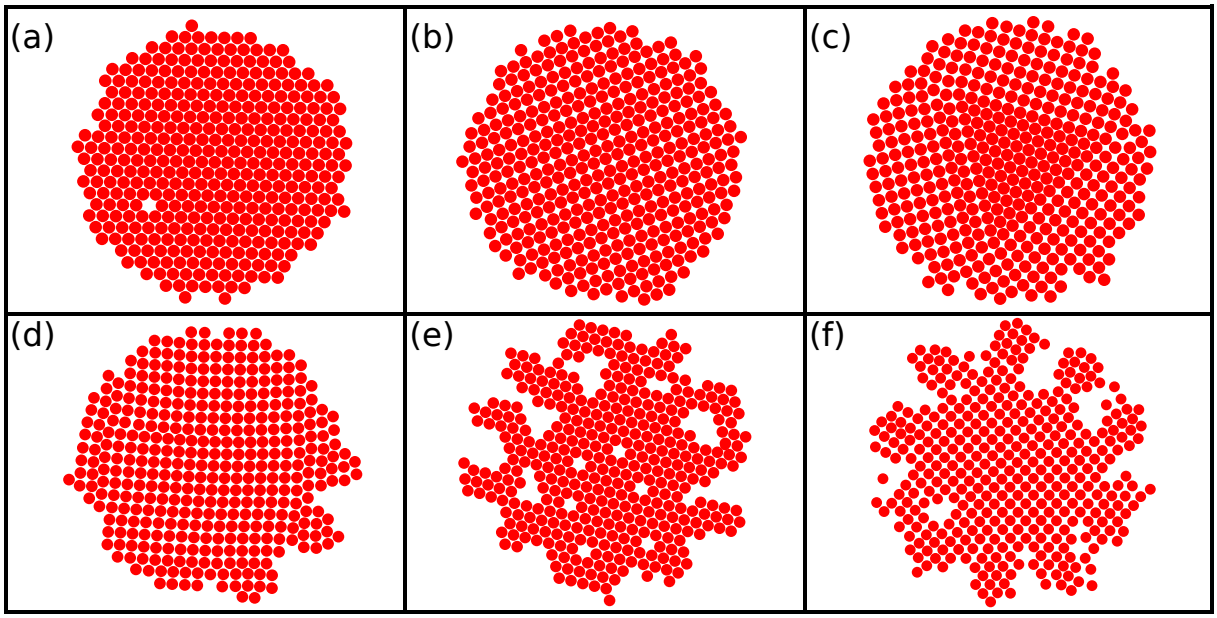

Figure 15 - Initial configuration obtained for systems with $N = 384$ particles, for (a) $R = 2.0$ and $\alpha = 1.00$, (b) $R = 2.0$ and $\alpha = 2.90$, (c) $R = 2.5$ and $\alpha = 1.6$, (d) $R = 2.5$ and $\alpha = 3.1$, (e) $R = 3.0$ and $\alpha = 2.4$, (f) $R = 3.5$ and $\alpha = 3.2$.

These structures were chosen because they all have different structural patterns, and, as explained in the introduction, the purpose of this work is to study the melting scenario of systems that hold more configurations than simply a compact triangular lattice, as it is the case of most melting studies. The set of values of the potential parameters, R and α, used for each of those simulations can be seen in the Fig. 15 caption.

3.3.2 Heating Method

Now that we have the initial configurations of the melting simulations, we can explain how to proceed with the heating process.

In order to simulate the melting process, we first scale our energy and length with ε and r_o, respectively, then we define the normalized temperature, given by $T^* = k_B T/\varepsilon$. The system temperature is set, initially, to $T_0^* = 0$ and, in the sequence, is slowly increased until $T_f^* = 30$. Good convergence was achieved for a normalized time step of $\varepsilon \Delta t/\gamma r_o^2 = 10^{-5}$. For each temperature T^*, we iterated the system 5×10^4 time steps before increasing the temperature by an amount of $\Delta T^* = 0.15$. Nowadays [66], in terms of experimental values, the colloidal radius are typically measured in nanometers (from dozens to hundreds).

3.4 STRUCTURES' CLASSIFICATION

Having the simulations been run, it is necessary to analyze the data provided by them. To do so, we use parameters capable of qualifying the configurations of the colloids, with values that create distinctions between these configurations. The purpose of these parameters is to analyze how they will change with the increasing temperature. The reason for not using thermodynamics to evaluate the results will be clear in chapter 4, as we will show the effect of the external potential on the melting scenario.

We separate this section in two parts, the first being for the explanation of the parameter used to classify microscopic structures, that is, the geometrical assembling between the colloids. The second part is about the classification of the macroscopic structures formed by the colloids, that is, the ornamental patterns that emerge from the self-assembly of the particles, such as the fringes seen in Fig. 15(e). In the end of the chapter, we shall use these classification methods to qualify the structures of Fig. 15.

3.4.1 Microscopic Structural Ordering

The microscopic structures emerge from the different symmetries of the particles' arrangement. In order to identify these symmetries, we define the parameter $\xi = \frac{1}{N}\sum_{i=1}^{N}\xi_i$, where

$$\xi_i = \frac{1}{(N_i-1)}\sum_{\{k,l\}}{}' \sin\theta_{\mathrm{kl}}^{\mathrm{i}}, \tag{26}$$

and N_i is the number of first neighbors of the i^{th} colloid. The sum is over the neighbors of colloid i, which are ordered in the counterclockwise direction, and θ_{kl}^{i} is the angle between the nighbor k and the next one l. The prime in the sum indicates that it does not take into account the term with the largest angle.

Fig. 16 presents a small cluster which illustrates a particle with its neighbors and the angles related to the calculation of ξ_i. In this example, one has $\xi_1 = (\sin\theta_{23}^{1} + \sin\theta_{34}^{1})/2$. The reason why we use the sine of the bond angles rather than the angles themselves is to better distinguish between, for instance, a perfectly triangular lattice from a rhombic lattice. In both cases, each particle has 6 neighbors forming 5 bond angles, so $\frac{1}{(N_i-1)}\sum_{\{k,l\}}\theta_{kl}^{i} = 300^{\circ}/5 = 60^{\circ}$ irrespective of the symmetry. However, in general, a rhombic lattice comprises two different bond angles:

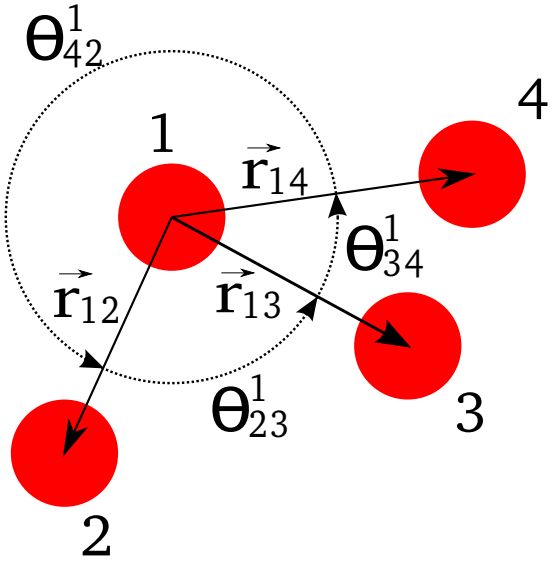

Figure 16 - Schematic representation of a hypothetical small cluster formed by four particles which are represented by circles and indexed by numbers from 1 to 4, where particles 2, 3 and 4 are neighbors of 1. the angle in the counterclockwise direction between the neighbor k and the next neighbor l is θ^1_{kl}. The angle θ^1_{42} is the largest one and therefore it is not used in the calculation of ξ_1.

θ, appearing 4 times, and ϕ, twice. Therefore, for a rhombic lattice with e.g. $\theta = 50^\circ$ and $\phi = 80^\circ$, $\xi_i = 0.839$, while $\xi_i = 0.866$ for the triangular lattice. In previous works such as Ref. [59], the ξ_i parameter was accurate enough to distinguish different microscopic states, that is, the triangular, square and mixed patterns.

The values of ξ_i for a given particle that belongs to a perfect triangular, square and mixed lattice are $\xi_i \approx 0.866$, $\xi_i \approx 1.00$ and $\xi_i \approx 0.92$, respectively. However, note that, in general, particles will not be in a perfect lattice due to thermal motion generated by the increase of temperature and due to some fringes in specific structures such as that of Fig. 15(f). Hence, we consider that if the value of ξ_i is in the range $0.85 \leqslant \xi_i < 0.89$, $0.89 \leqslant \xi_i < 0.96$ and $0.96 \leqslant \xi_i \leqslant 1.00$, the i^{th} particle belongs, respectively, to a triangular, mixed or square lattice. We define the value of ξ_i for a solitary particle as zero.

One might ask why we do not use the generic q parameter metioned in the introduction (Eq. 4). The answer is that the parameter ξ has some characteristics that are suitable for our structure analysis. For instance, if we were to use q, it would be necessary to define and use three parameters at once, $q_{triangular}$, q_{square}, q_{mixed}, one for each type of symmetry. This would not be pratical since in our system the microscopic arrangements before a complete melted stage. However, by solely using ξ, we are able to identify the three different symmetries usually found

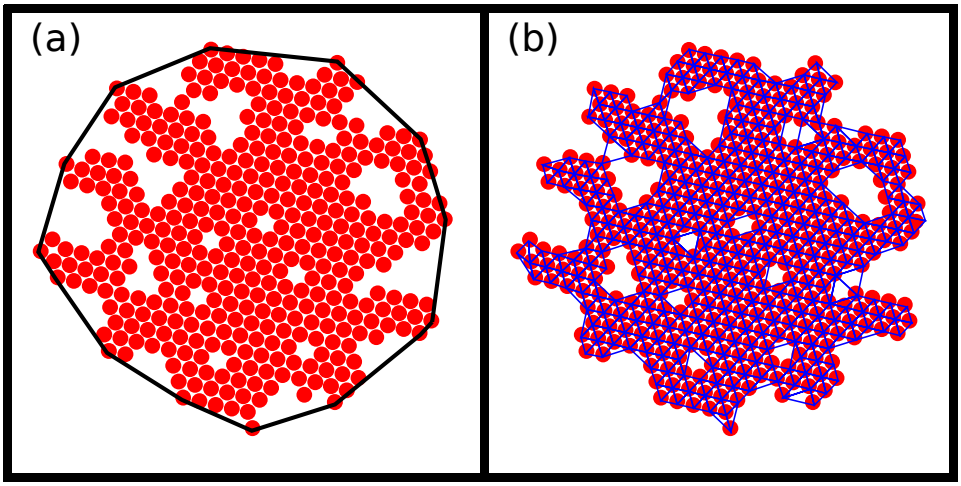

Figure 17 - Convex hull (a) and Delaunay triangulation (b) of the representative cluster with $N = 384$ particles obtained for $R = 3.0$ and $\alpha = 2.4$.

in our system. Moreover, its definition allows us to identify the microscopic order in the border of the cluster, a task which is not easy with the use of q because it takes into account a fixed neighbors number.

3.4.2 Macroscopic Structural Ordering

We have already commented in the introduction that the colloidal particles are able to self-assemble in complex structures exhibiting some interesting macroscopic properties. Examples of such macroscopic states are those where the cluster structures present fringes in their outer boundaries or a crystalline inner region perforated by voids.

Fig. 15(e) displays a configuration obtained trough the annealing process for the particular case of $R = 3.0$ and $\alpha = 2.4$. We can see that such a cluster is perforated by voids and presents fringes on its outer boundaries and its dominant ordering is that of a triangular type. On the other hand Fig. 15(a) represents a core crystalline triangular cluster, which is obtained for different parameters' values, $R = 2.0$ and $\alpha = 1.00$. Even though the ξ parameter for these two cases has the same value, that of a triangular arrangement, the structures are different from each other.

In order to distinguish between these types of configurations, we have defined the quantity η. The latter is defined as the ratio between the area occupied by the colloids, A_p, and the area delimited by the smallest convex polygon that contains the entire cluster, A_c, i.e., the convex hull. In calculating A_p, we first use the Delaunay triangulation [67] to generate the set of trian-

α	R	**Microscopic Order**	**Macroscopic Patterns**
1.00	2.00	Triangular	compact
2.90	2.00	Mixed	compact
1.60	2.50	Triangular and squared	compact
3.10	2.50	Squared	None
2.40	3.00	Triangular	Fringes and holes
3.20	3.50	Squared	Fringes

Table 2 Set of parameters used to generate the specific structures depicted in Fig. 15 with their correspondents macroscopic properties.

gles with vertices on the colloidal centers, and, second, we discard those edges of the triangles that are larger than two colloidal diameters. The total area of the remaining triangles gives the quantity A_p. An example of such triangulation can be seen in Fig. 17(b), while Fig. 17(a) shows the convex hull of such cluster.

The ground state ratio, η, for the case of Fig. 15(a) is $\eta \approx 0.94$, whereas for the case of Fig. 15(e) is $\eta \approx 0.70$, therefore this method is useful in separating fringed clusters from the more dense ones.

Lastly, we organize the classifications of the initial structures used in our simulations, for didactic purpose, in Table. 2.

4 MELTING PROCESSES ANALYSIS

For this chapter, we will focus on the analysis of the data provided by the simulations. This will be done by the use of the microscopic and macroscopic structures' classification method introduced in chapter 3. The investigation of the dynamical processes related to the configurations shown in Fig. 15 provided us with a rich scenario. Due to this fact, and in order to make our explanation more didactic, we found convenient to divide this chapter into three sections. In the first section, we describe quantitatively how the microscopic ordering of the clusters is changed by the increasing of temperature. To do so, we calculated the ξ parameter, which gives information about the cluster's symmetry. By doing this, We will show that during the melting process, particles are able to swing between some different microphases and, at high temperature regime, the system loses its angular ordering while still preserves its radial inter-particle confinement. In the second section , we investigate whether the system in question exhibits spatial inhomogeneities in the melting process. In the last section, we focus our investigation on the macroscopic analysis of melting and show that the fringes stability demonstrated to be higher than the one found in compact clusters.

4.1 PHASE TRANSITION OF THE MICROSCOPIC ORDERING

In this section, we investigate the change of the microscopic ordering patterns due to the increasing of temperature for different values of the system parameters α and R. In particular, we will try to answer the following questions: What happens to the triangular, square and mixed orderings due to thermal effects? Does the interaction potential present any effects at the high temperature regime? How the confining potential influences the melting process? In order to answer these questions it is appropriate to analyze the melting of the system over different scales, that is, first considering the melting regime at low temperatures and, in the sequence, at high temperatures.

4.1.1 Low Temperature Regime

To make the simulations results clearer, we define and calculate the following radial quantity

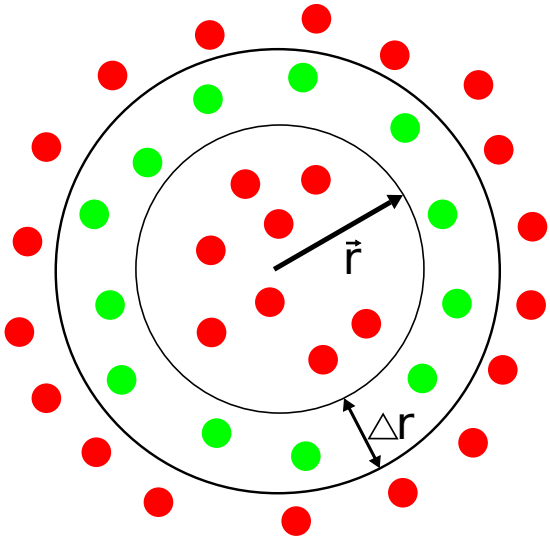

Figure 18 - Schematic representation of the ring used to determine the particles considered in the calculation of $\xi(r)$. Only the particles within the ring (green colored disks) are taken into account for the calculation of $\xi(r)$.

$$\xi(r) = \frac{1}{n}\sum_{i=1}^{n}\xi_i, \tag{27}$$

where ξ_i is the microscopic parameter of particle i defined in Eq. 26. In Eq. 27, the sum takes into account the n particles within a ring of thickness $\delta r = 0.1$, centered at the origin and whose internal radius is r. Fig. 18 shows a representation of this ring, in order to help to understand how we must calculate $\xi(r)$ for a given cluster. Note that only the values of ξ_i related to the particles belonging to the ring (blue colored disks) are taken into account for the calculation of $\xi(r)$.

We can now analyze $\xi(r)$ by taking the time average of this parameter. In Fig. 19 we display $\langle\xi(r)\rangle_t$, where brackets stands for a time average, as a function of the cluster's radius at different temperatures for different parameters R and α. First thing to note is that for zero temperature (green squares) we have the ground states of the systems, hence the values of $\langle\xi(r)\rangle_t$ in this temperature correspond to the structures in Fig. 15.

In the construction of Fig. 19 we have set that an isolated particle has a ξ value equal to zero. Therefore, we can conclude that, for increasing values of temperature, particles located near the clusters' border are the first ones to become isolated. We also note that, as the temperature increases, the quantity $\langle\xi(r)\rangle_t$ decreases gradually with the increasing of the radius. This suggests that before becoming solitary, particles near the border start to have less neighbors,

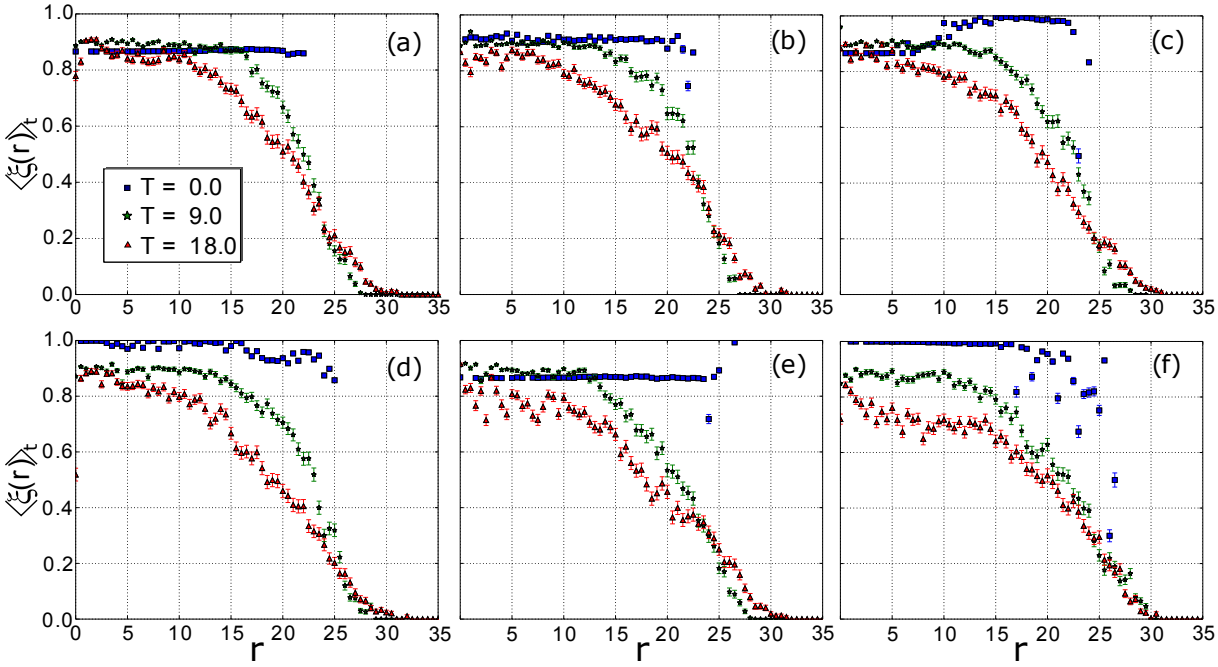

Figure 19 - Mean value of ξ as a function of the cluster radial size for temperatures $T^* = 0$ (blue squares), $T^* = 9$ (green stars) and $T^* = 18$ (red triangles) for the cases (a) $R = 2.0$ and $\alpha = 1.0$, (b) $R = 2.0$ and $\alpha = 2.9$, (c) $R = 2.5$ and $\alpha = 1.6$, (d) $R = 2.5$ and $\alpha = 3.1$, (e) $R = 3.0$ and $\alpha = 2.4$, (f) $R = 3.5$ and $\alpha = 3.2$.

which leads to the formation of larger bond angles, and therefore, smaller values of the terms $\sin\theta_{kl}^{i}$ in Eq. 26. Fig. 20 shows a snapshot of the upper border of the cluster for the parameters $R = 2.0$, $\alpha = 1.0$ and $T^* = 10.0$. Notice that the highlighted particles, which are colored in green (light gray), have at least one pair of neighbors forming a bonding angle larger than 90 degrees.

From Fig. 19 we can see that the microscopic ordering formed by the most internal particles (the clusters' core) also changes with the increasing of temperature. Indeed, as temperature raises, the value of $\langle \xi(r) \rangle_t$ changes, therefore, demonstrating that thermal energy can lead to a fluctuation of the microscopic ordering. Figs. 21(a) and 21(b), corresponding to the system parameters $R = 2.5$ and $\alpha = 3.1$, show the particles' configurations, respectively, for temperature values equal to $T^* = 0.0$ and $T^* = 2.25$. Notice that, for Fig. 21(a), the inner particles start, predominantly, in a square lattice, while, in Fig. 21(b), for a larger temperature, particles evolved to a mixed type lattice.

In order to understand the melting processes involving the fluctuations of crystalline structures we decided to calculate the percentages of triangular, mixed and square lattices as a function of temperature. The result of this calculation is presented in Fig. 22 for the different values

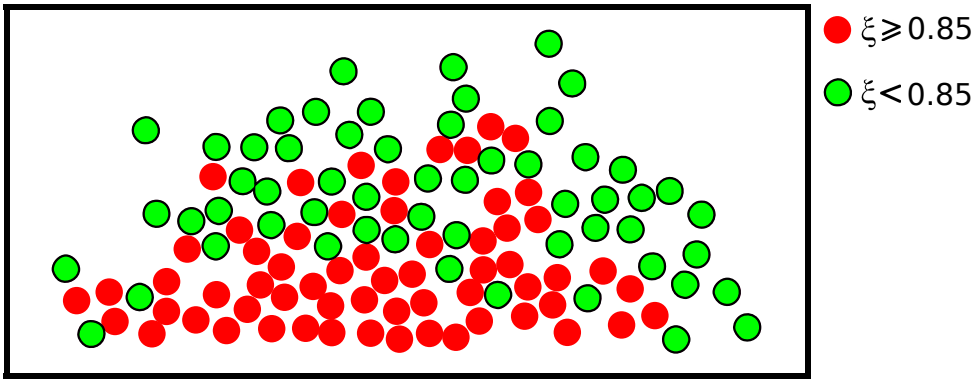

Figure 20 - Amplified image of the upper part of the cluster shown in Fig. 15(a) ($R = 2.0$ and $\alpha = 1.0$) for an elevated temperature $T^* = 10.0$. Particles having $\xi < 0.85$ and $\xi \geq 0.85$ are indicated, respectively by green and red disks.

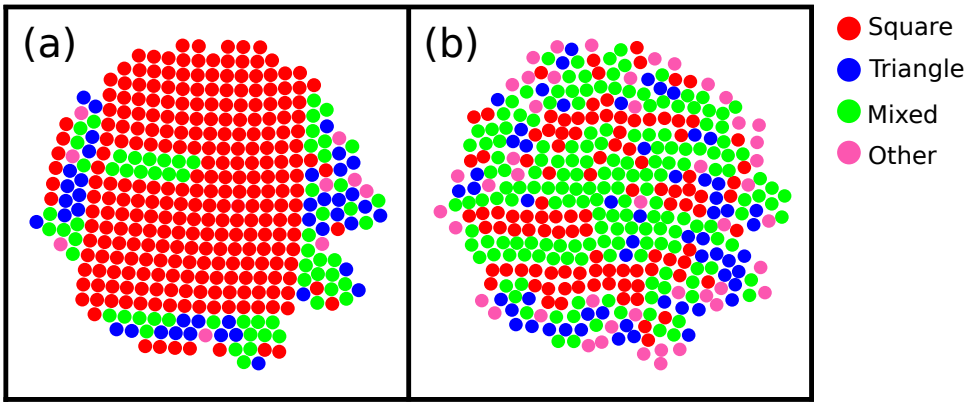

Figure 21 - Minimum energy configurations for the system with $R = 2.5$, $\alpha = 3.1$, $N = 384$, and temperatures (a) $T^* = 0.0$ and (b) $T^* = 2.25$. The disks' colors indicate the lattice in which the particles belong as shown in the legend.

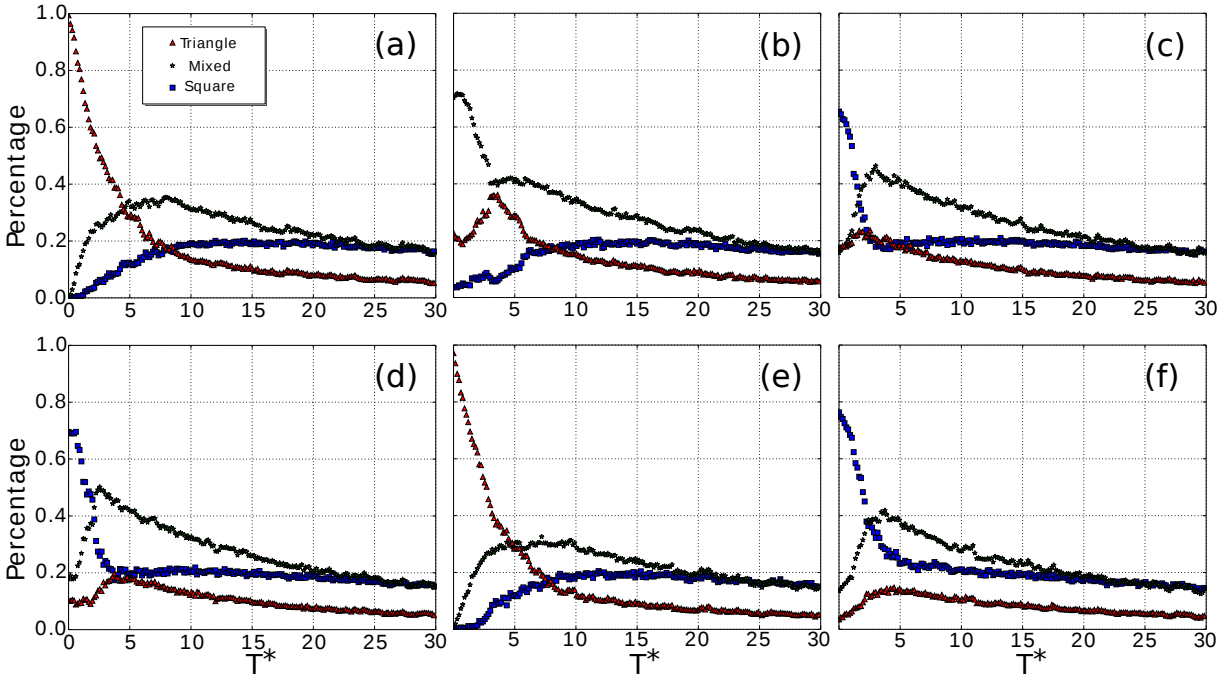

Figure 22 - Mean value of the percentages of triangular, mixed and square structures as a function of temperature for the cases (a) $R = 2.0$ and $\alpha = 1.0$, (b) $R = 2.0$ and $\alpha = 2.9$, (c) $R = 2.5$ and $\alpha = 1.6$, (d) $R = 2.5$ and $\alpha = 3.1$, (e) $R = 3.0$ and $\alpha = 2.4$, and (f) $R = 3.5$ and $\alpha = 3.2$.

of R and α. We can see that, for high enough temperatures, all the systems present a similar behavior, that is, the lattices' percentages converge for the same values. On the other hand, at low temperatures, such percentages depend strongly on the R and α parameters of the systems. Therefore, we can conclude that the interaction potential between particles is, in fact, what contributes most to the microscopic ordering.

Fig. 22(a) presents the percentage of triangular (triangles), square (squares) and mixed (stars) structures as a function of temperature for a system whose zero temperature configuration holds a triangular microscopic ordering. We can see that, at the low temperature regime, the increasing of temperature leads to a decreasing in the number of triangular structures concomitantly with the growth in the number of square and mixed structures. Note that Fig. 22(e) presents, basically, the same phenomenon in Fig. 22(a). This fact is not a surprise, since the zero temperature order related to the latter two figures is the triangular ordering.

The reason for the increasing of the square and mixed structures is revealed by our molecular dynamics simulations. Due to thermal motion, full lines of particles become able to dislocate and then to occupy empty spaces that occasionally appear. Fig. 23(a) shows a schematic representation of the particles' dislocation observed in the melting of Figs. 15(a) and 15(e). This

motion illustrates one of the main mechanisms responsible by the appearance of the mixed arrangement, that is, a dislocation process. This mechanism explains why the mixed configurations are formed first, that is, as temperature slowly increases, particles subtly dislocate, in a way that the first formed squares are surrounded by triangles, therefore forming a mixed lattice. Still, in both previous cases, we notice that when temperature achieves the value $T^* \approx 5$, the percentage of mixed patterns (stars data) begin to dominate the ordering of the clusters.

Fig. 22(b), which corresponds to the melting process of the configuration shown in Fig. 15(b), presents an interesting phenomenon. Note that, at the initial stage of the melting, the percentage of mixed structures, which was initially dominant, falls very fast to almost half its value, while the number of triangular structures rapidly increases. The process undergone to achieve this transition is presented in Fig. 23(b).

The melting processes related to the systems where the square patterns are initially predominant is revealed from Figs. 22(c), 22(d) and 22(f). Note that, the percentage of squares falls very rapidly and are surpassed by the mixed structures. The microscopic behavior responsible for such a transition also becomes clear from our molecular dynamics simulations, and corresponds to the scheme shown in Fig. 23(c). Note that this process also creates some triangular structures, which corresponds to the small increment in the percentage of triangles. The percentage of squares decreases very rapidly until a value around 20%. After that, such a percentage has a much smoother drop since the effect of the interaction potential is minimized by the kinetic energy.

These types of microscopic changes in the low temperature regime are quite interesting, because the process undegone by the colloids resembles shear slips [68] as we can see in Fig.23. It's also very interesing the polystructures created by it, that is, there is a competition between the different microscopic arrangements. Such structures competitions have been observed in nucleation of crystals in three dimensions (see Refs. [69],[70]).

4.1.2 High Temperature Regime

For temperatures higher than $T^* = 15$, we can verify, from Fig. 22, that all systems exhibit approximately the same behavior. This fact occurs due to the breakdown of long-range ordering between particles. However, despite such a break in symmetry, our simulations demonstrate that the system still presents ordering. Indeed, in such a realm where short-range interactions

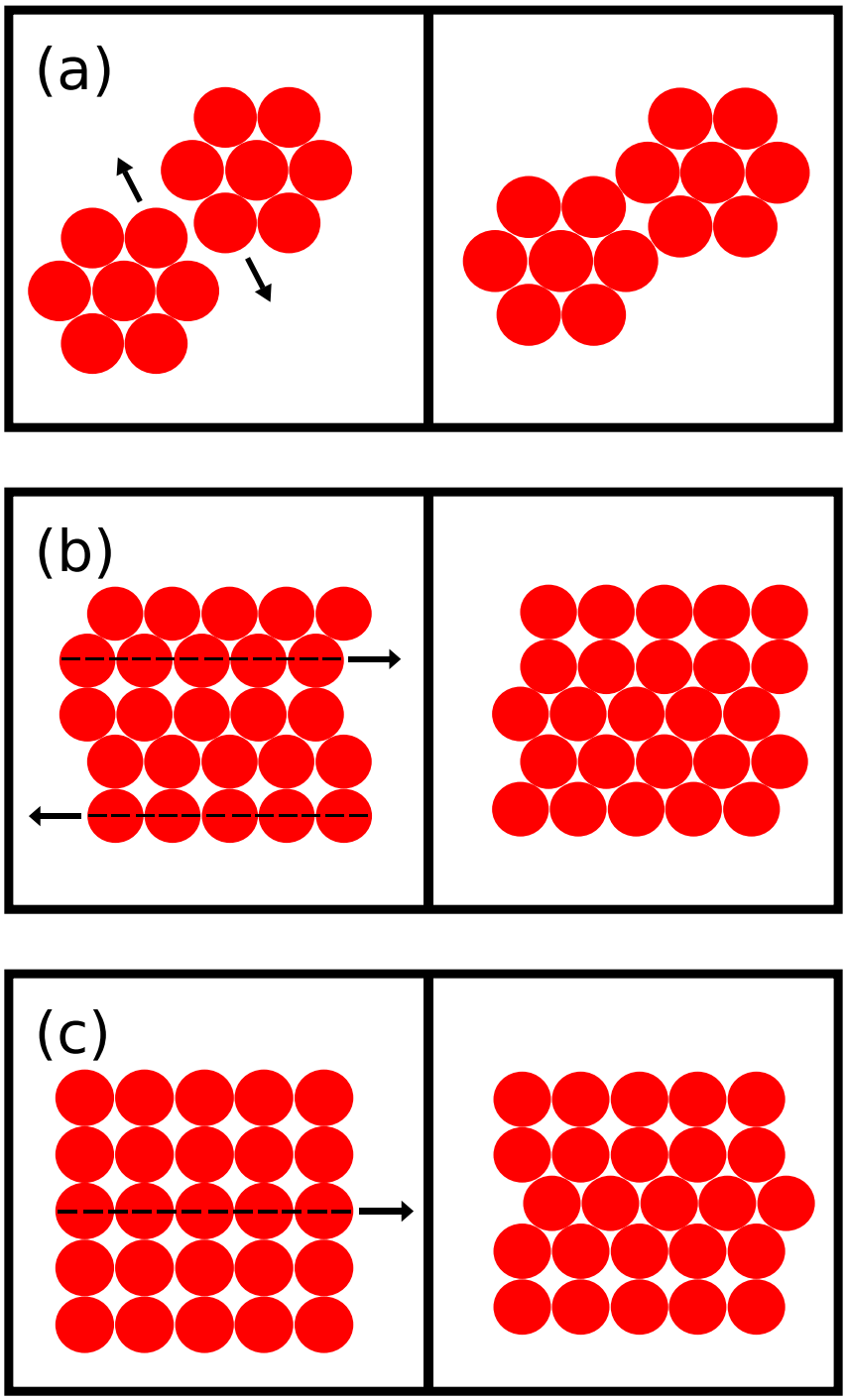

Figure 23 - Representations of the various displacements of particle lines related to the transitions between the phases (a) triangular to mixed, (b) mixed to triangular and square, and (c) square to mixed and triangular.

Neighbor N°/R;α	2.0;1.0	2.0;2.9	2.5;1.6	2.5;3.1	3.0;2.4	3.5;3.2
2	27.159%	26.747%	27.179%	27.234%	27.665%	27.995%
3	21.270%	21.054%	20.461%	20.051%	19.323%	18.394%
4	9.489%	9.365%	8.695%	8.189%	7.399%	6.474%
5	1.708%	1.674%	1.493%	1.379%	1.096%	0.917%
6	0.006%	0.006%	0.005%	0.004%	0.003%	0.002%

Table 3 - Average percentage of the number of neighbors for the case of high temperatures ($25.0 \leqslant T \leqslant 30.0$) for all six set of parameters.

predominate, we could verify, as will be demonstrated in the following, that the dynamics is governed by the continuous emergence and destruction of small aggregates of particles.

We can see from Fig. 22 that, for $T^* \geq 25$, the percentages of mixed, square and triangular aggregates become around 17%, 16% and 6%, respectively. The fact that these percentages achieve such values is no mere coincidence. Actually, we will, in this section, show that this result is proper of high temperature systems where the interaction potential has low influence on the clusters orientational ordering.

From our molecular dynamics simulations, performed for high temperatures, we were able to compute the percentage of particles having a specific number of neighbors. These results are presented in Table 3 for several values of the parameters R and α. We can see from this latter that most particles have two neighbors. In fact, the percentage of particles with two neighbors is around 27% for all parameters. This proportion gradually decreases with increasing number of neighbors. We can see, for example, that the percentage of particles having 6 neighbors is around 0.005%, which is negligible compared to the other values.

A particle with $n-1$ first neighbors must belong to a cluster with at least n particles. Such a particle may belong to a triangular, square, or mixed arrangement depending on the interaction potential parameters and as well as the temperature. At high temperatures we conjecture that there is no more angular order between particles. In order to test this hypothesis and, at the same time, obtain the probability that a particle belongs to one of the given lattices in question, we have performed Monte Carlos simulations.

The procedure related to Monte Carlo simulations consists of defining a specific number of particles for a given cluster, and then, choosing a particle, which we call central particle, for which we calculate the quantity ξ. The other particles are neighbors of the central particle and,

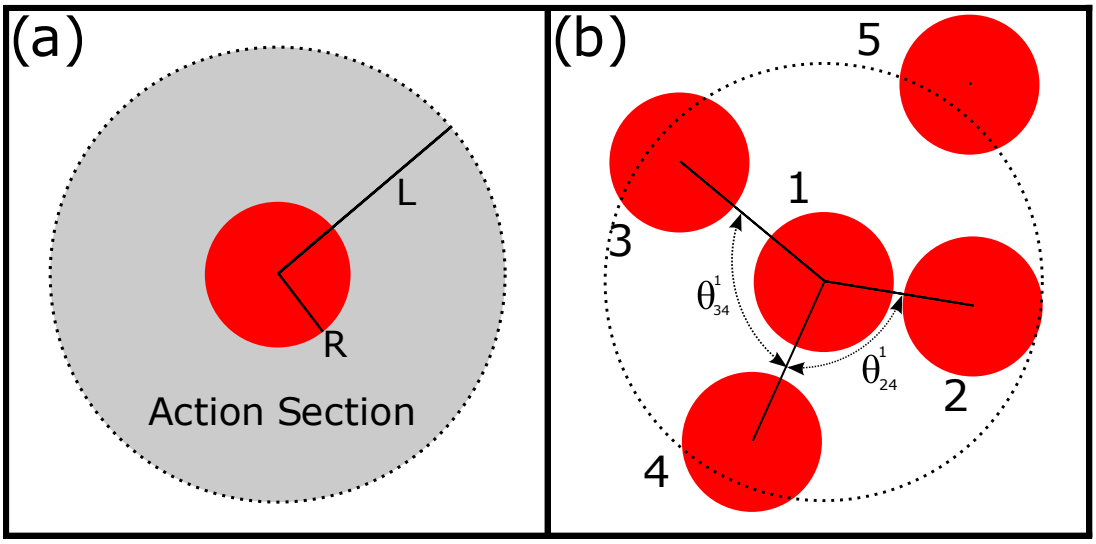

Figure 24 - Scheme showing how the quantity ξ was calculated in our Monte Carlo simulations. (a) A central particle is represented by a red colored disk. L represents the greatest distance that a second particle can have from the central one so that both can be considered neighbors. The region delimited by the circle of radius L is called the action section. (b) Representation of a cluster containing one central particle and four other surrounding particles. Note that only the particles of indexes 2, 3 and 4 are within the action section, and therefore, are neighboring of the central particle. The fifth particle is not a neighbor of the central particle and therefore does not contribute to the calculation of ξ. The angles θ^1_{24} and θ^1_{34} contributing to the calculation of ξ are also shown.

for didactic purposes, we call them lateral particles. In executing the simulation we sort the random positions of the lateral particles considering that all permitted states are equally likely and taking into account two constraints. The first constraint is that no lateral particle can be at a distance greater than L from the central particle, otherwise they would not be a neighboring particle. The second restriction is that no pair of particles can be at a distance less than $D = 2R$, as this would lead to an overlapping of two particles whose potential are hard.

Fig. 24(a) shows a scheme where the central particle is displayed in red, and the gray circular area, which is surrounded by a dotted circle, represents the action section, that is, the area wherein any particle is considered a neighbor of the central particle. In fact, the distance from the dotted circle and the central particle is L, therefore any other particle whose center is within the action section is, by our definition, a neighbor of the central particle. Fig. 24(b) shows a scheme where the central particle is surrounded by four other particles. However, note that only three particles, that is, the particles labeled by the numbers 2, 3 and 4 are within the action section, and therefore, are considered neighbors of the central particle. The most external particle,

Neighbor Number	Triangular	Mixed	Square
2	7.3%	17.0%	25.5%
3	14.9%	42.7%	31.4%
4	10.7%	62.0%	26.0%
5	39.2%	58.2%	0.0%
6	5.3%	0.0%	0.0%

Table 4 - Set of the structures probabilities obtained in the Monte Carlo simulations with random positions for different number of neighbors.

labeled by the number 5, has its center outside the action section and then is not considered a neighbor of the central particle. In order to calculate the quantity ξ and the bond angles we followed the procedures explained in chapter 3 (see Fig. 16).

Our Monte Carlo simulations computed the value of ξ over ten million times for each neighbor number. Table 4 presents the probability of a given particle having a specific number of neighbors be part of a triangular, square and mixed arrangement.

Now, we are able to calculate the expected probabilities of a given particle to belong to a mixed, square or triangular lattice under the consideration that the angular particle orientation is random. These results are obtained from Tables 3 and 4 by means of a weighted average of their data. As an example, we have that the expected probability of a triangular aggregate is given by

$$P^{tri} = \sum_{i=2}^{6} p_i \cdot p_i^{tri}, \tag{28}$$

where p_i is the probability that a given particle has i neighbors and p_i^{tri} is the probability that a cluster with $(i+1)$ particles forms a triangular arrangement. We have compiled the results of such calculations for the different lattices in Table 5.

Finally, we present in Table 6 the quantities p^{tri}, P^{mix} and P^{sqr}, which are, respectively, the probabilities of a triangular, mixed and square arrangement be formed. These results were obtained from our molecular dynamics simulations. A comparison between Tables 5 and 6 reveals a good agreement of results, meaning that, at high temperatures, there is in fact no angular orientation. The latter fact demonstrates why the data in Fig. 22, for the high temperature regime, converge to the same values, independently of the systems' parameters.

Percent/R;α	2.0; 1.0	2.0; 2.9	2.5; 1.6	2.5; 3.1	3.0; 2.4	3.5; 3.2
P^{tri}	6.843%	6.754%	6.555%	6.399%	6.126%	5.843%
P^{mix}	20.607%	20.347%	19.646%	19.099%	18.206%	17.186%
P^{sqr}	16.065%	15.859%	15.609%	15.363%	15.038%	14.590%

Table 5 - Monte Carlo simulations percentages of triangular, mixed and square aggregates for the case of high temperatures ($25.0 \leqslant T \leqslant 30.0$) for all six set of parameters.

Percent/R;α	2.0; 1.0	2.0; 2.9	2.5; 1.6	2.5; 3.1	3.0; 2.4	3.5; 3.2
P^{tri}	$(6 \pm 1)\%$	$(6 \pm 1)\%$	$(5 \pm 1)\%$	$(5 \pm 1)\%$	$(5 \pm 1)\%$	$(4 \pm 1)\%$
P^{mix}	$(17 \pm 3)\%$	$(16 \pm 3)\%$	$(16 \pm 3)\%$	$(15 \pm 3)\%$	$(15 \pm 3)\%$	$(14 \pm 3)\%$
P^{sqr}	$(16 \pm 2)\%$	$(15 \pm 2)\%$	$(16 \pm 2)\%$	$(15 \pm 2)\%$	$(15 \pm 2)\%$	$(14 \pm 2)\%$

Table 6 -Molecular dynamics simulations results of the average and standard deviation of the percentages of triangular, mixed and square aggregates for the case of high temperatures ($25.0 \leqslant T \leqslant 30.0$) for all six set of parameters.

4.2 CONFINED MELTING

Finite systems of small dimensions usually show inhomogeneous melting. In such an inhomogeneous process, the dynamics of the particles depend strongly on their spatial location. In this way, a natural question we can ask is whether, for the system in question, there is a difference in the melting process between the innermost regions of the cluster and the one near the edge.

Fig. 25 shows the lattice percentages as function of temperature for the most internal region of the cluster. In order to determine the different lattices percentages we have calculated the quantity ξ in a similar way to what we did in Fig. 22. The inner region we take into account is bounded by a circle of radius $R^{circ} = 5.5$ centered on the origin. This value is approximately equal to a quarter of the radius of the cluster at zero temperature.

A brief comparison between Figs. 22 and 25 indicates that they are qualitatively very similar. Indeed, we can see that both figures indicate the same general types of phenomena with the exception of a few small details. Such details, which have been covered up when we analyzed the melting as a whole, will be discussed in the sequence.

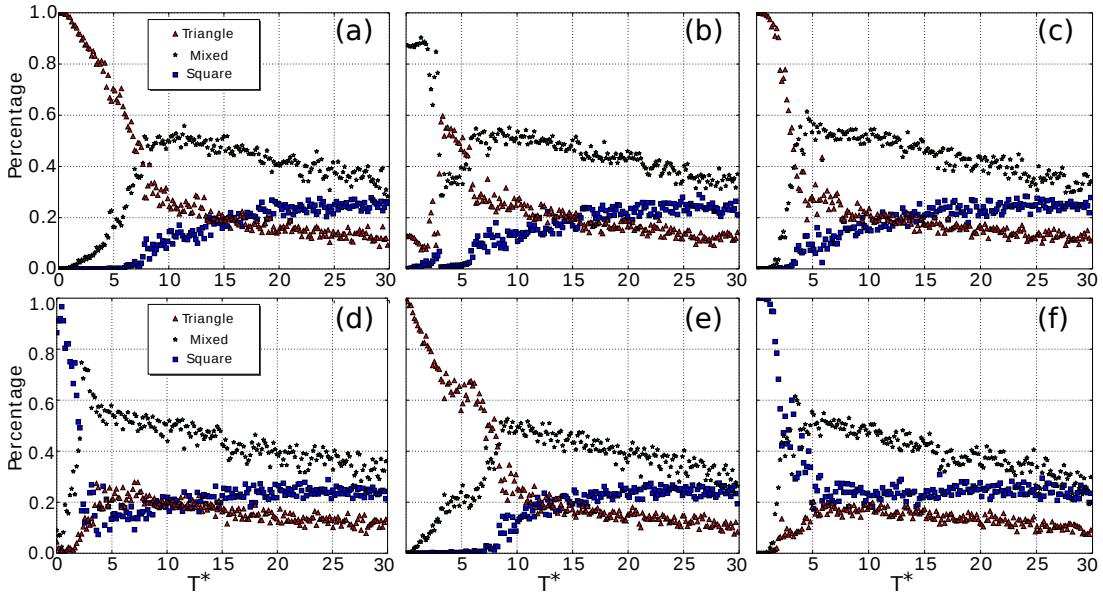

Figure 25 - Mean value of the percentage of triangular, mixed and square structures calculated for the particles within the centered circumference of radius $R_{cir} = 5.5$, as a function of the temperature for the cases (a) $R = 2.0$ and $\alpha = 1.0$, (b) $R = 2.0$ and $\alpha = 2.9$, (c) $R = 2.5$ and $\alpha = 1.6$, (d) $R = 2.5$ and $\alpha = 3.1$, (e) $R = 3.0$ and $\alpha = 2.4$, (f) $R = 3.5$ and $\alpha = 3.2$

Figs. 25(a) and 25(e) show a good quantitative agreement, which is expected, since they are related to configurations that assemble almost the same characteristics near the center. This latter fact can be clearly seen from Figs. 15(a) and 15(e), where the cluster core is, predominantly, made up by a triangular lattice. Most importantly, note that the initially non-existent lattices start to occur only at relatively higher temperatures. This is what happens with the square lattice, which starts to grow at the temperature $T^* = 8.0$ as we can see from Figs. 25(a) and 25(e). In contrast, from Figs. 22(a) and 22(e), we see that the appearance of the square lattice is almost immediate for increasing values of temperature. Therefore, we conclude that the appearance of the square lattice starts at the clusters edge. A similar situation can be found for the other system parameters. For example, from Figs. 25(d) and 25(f), we can find a delay in the growth of the triangular lattice in the region near the center.

The dynamic behavior revealed by Figs. 22(c) and 22(c) shows a qualitative agreement between them, with only one change concerning the percentage values of the triangular and square lattices. Such an interchange is in accordance with the characteristics presented in the configuration of Fig. 15(c). In this latter the outermost region is composed of a square lattice while the innermost is composed of a triangular lattice.

The lattices structures are found to be more resistant to the temperature rising in the inner-

most region of the cluster than in the outermost region. To conclude this, it is enough to verify from Figs. 25(b) and 25(f) that, respectively, the initial percentages of the mixed and squared lattices do not fall immediately to increasing temperature values. On the other hand, an immediate decrease of such lattices at the edge clusters can be verified when we take into account Figs. 22(b) and 22(f). A similar phenomenon is found for the systems presented in Figs. 15(a) and 15(c), but now for the triangular lattice, as shown in Figs. 25(a) and 25(c).

Finally, we can conclude that the melting temperature of the center is greater than that at the edge of the cluster. This fact is caused by the effect of the external potential which tends to increase the pressure in the innermost regions of the cluster. This means that defining a critical temperature for the whole cluster is not plausible, since the melting temperature depends on the radial distance from the center.

4.3 PHASE TRANSITIONS OF THE MACROSCOPIC ORDERING

Now, we are going to analyze the effects caused by the melting processes over ornamental patterns of the clusters. We consider the case where the border of the cluster is formed by fringes while its interior is spanned by a crystalline arrangement. In practice, we investigate the main characteristics relative to the dynamical changes played by the fringed and compact clusters as a function of the raising temperature. To do so, we computed the averaged time of the quantity η, which was defined in chapter 3 (see Fig. 17) as the ratio between the altered Delaunay triangulation and the convex hull areas.

This quantity η indicates how dense the cluster is, that is, the closer the value of η is from the unity, the more compact the cluster is, and vice versa. Indeed, if the value of η is close to unity, then the convex hull and the altered Delaunay triangulation areas are close to each other. On the other hand, a value of η close to zero is characteristic of a cluster where particles in the border are dispersed, since, in this case, the convex hull area becomes larger than the triangulation area. This last situation will always be achieved with the increasing of temperature, since, as we have already commented, particles on the border are the first ones to fall off the cluster.

Fig. 26 presents the time average $\langle \eta \rangle_t$ as a function of temperature for the configurations with $R = 2.0$ and $\alpha = 1.0$ (blue squares), $R = 2.5$ and $\alpha = 3.1$ (green stars) and $R = 3.0$ and $\alpha = 2.4$ (red triangles). We can see that, the values of η, relative to the fringed cluster (red triangles), remain constant for a longer temperature range when compared to the values of η

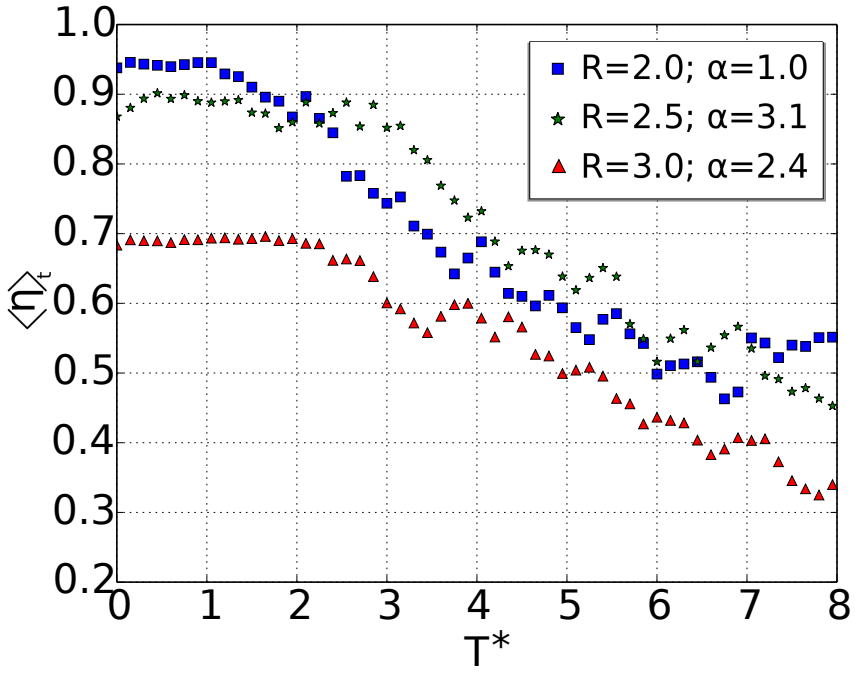

Figure 26 - Time average of η, defined by the ratio between the areas of the convex hull and altered Delaunay triangulation. The cases $R = 2.0$ with $\alpha = 1.0$ (blue) and $R = 2.5$ with $\alpha = 3.1$ (green) represent the compact systems where the ground states are triangular and squared, respectively, whereas the case $R = 3.0$ with $\alpha = 2.4$ (red) represents the systems with fringes appearing in the ground state.

computed to the fringed clusters (see the blue and green data in Fig. 26).

Such a fact is interesting, since it reveals that fringed clusters withstand more to the initial stage of the melting process than clusters without fringes. In fact, fringes are able to minimize the cluster energy to a point that particles belonging to it can sustain some extra thermal energy and still remain attached to the cluster.

5 CONCLUSIONS

In this dissertation we have investigated the dynamical processes of a $2D$ system of colloidal particles interacting via a quasi-square well potential and confined by a parabolic external trap. The present investigation took advantage of previous work done by Costa Campos et al [28], in which they performed a detailed study involving the lower energy configurations of such colloids. In this latter, it was possible to identify two main forms of particle organizations, which we called here microscopic and macroscopic orderings. These orderings were separately studied in the melting simulations. With respect to the type of potential used in the system, we expected to obtain a rich melting scenario, since the potential was quite complex and responsible for the formation of many different structures.

With the intention to introduce a little bit about simulations of colloidal systems, we discussed the essence of molecular dynamics and Monte Carlo methods. We also introduced the basic notion of $2D$ melting theories, in particular the KTNHY theory, where it is expected to be observed a two-step melting with a stable hexatic phase. Such phase was not observed in our simulations due to the fact that the potential used has a significant long attractive part when compared to the potentials used to derive the KTNHY theory. However, we were able to observe what seems to be a two-step melting, where in low temperature regime, the microscopic phases of the systems change before the colloids loose their angular correlations.

In order to describe the various melting stages of the system and its behavior in terms of temperature and the clusters' structural characteristics, we made use of both, molecular dynamics and Monte Carlo simulations. The latter was essential to explain the proliferation of small particle agglomerates induced by increasing temperature. We have also shown that, due to the external confinement, the melting of the system is inhomogeneous, that is, the region closer to the center is more resistant to the temperature raise than that located near the clusters' border.

Our molecular dynamics simulations demonstrated that within the low temperature regime, small fluctuations of thermal energy are sufficient to induce phase transitions involving two different crystalline orderings. For instance, for the set of parameter $R = 3.5$ and $\alpha = 3.2$, we found that the increasing in temperature can bring the system from a square to a mixed lattice. Similarly, for the case $R = 3.0$ and $\alpha = 2.4$, we could verify the transition involving the passage from the triangular to the mixed phase. Moreover, the microscopic mechanisms mediating these phase transitions were presented and discussed in details in chapter 4. These

mechanisms resembled shear slips, were lines of particles would stress each other to movement. Not only that, but the coexistence of different microscopic arrangements is quite interesting, for they represent a competition between the structures to minimize the total energy.

Lastly, we investigated the effects of temperature over particles located near the border of the clusters. Our molecular dynamics simulations showed that particles present on the borders of fringed clusters form a more stable structure than that seen on the borders of compact clusters. Indeed, it was seen that particles on the periphery of compact clusters could get off the main core of the cluster at a much lower temperature than that on the periphery of fringed clusters.

It is important to analyze the melting of these finite systems with different microscopic states, since the analytical studies of them are still being researched. The spatial inhomogeneity in the melting process makes the definition of a critical temperature a very arbitrary task, however, with the use of simulation methods, like molecular dynamics, it is possible to analyze the melting process even at microscopic scales.

BIBLIOGRAPHY

[1] J. B. Jones, J. V. Sanders, and E. R. Segnit, Nature **204**, 990-991 (1964).

[2] Frimmel, Fritz H., von der Kammer, Frank, Flemming, Hans-Curt. *Colloidal Transport in Porous Media.* Springer, 2007.

[3] A. Einstein, Ann. Phys. **17** 549 (1905).

[4] R. C. Desai and R. Kapral. *Dynamics of Self-organized and Self-assembled Structures*. Cambridge University Press (2009).

[5] J. Zhang. *Self-assembled nanostructures*, volume 2. Springer (2003).

[6] G. Malescio and G. Pellicane. Stripe patterns in two-dimensional systems with core-corona molecular architecture. Phys. Rev. E **70**, 021202 (2004).

[7] Y. Huang and J. Yang. *Novel colloidal forming of ceramics*. Springer (2010).

[8] H. J. Zhao, V. R. Misko, and F. M. Peeters, Phys. Rev. E **88**, 022914 (2013).

[9] H. J. Zhao, V. R. Misko, and F. M. Peeters, New J. Phys. **14**, 063032 (2012).

[10] S. A. Mallory and A. Cacciuto, Phys. Rev. E **94**, 022607 (2016).

[11] F. Schweitzer. *Brownian Agents and Active Particles: Collective Dynamics in the Natural and Social Sciences.* Springer, 2003.

[12] Hai Pham Van, Andrea Fortini, and Matthias Schmidt, Phys. Rev. E **93**, 052609 (2016).

[13] Peter J. Lu, Jacinta C. Conrad, Hans M. Wyss, Andrew B. Schofield, and David A. Weitz, Phys. Rev. Letters **96**, 028306 (2006).

[14] Ronen Zangi and Stuart A. Rice, Phys. Rev. E **61**, 1 (2000).

[15] Peter J. Collings and Michael Hird. *Introduction To Liquid Crystals: Chemistry and Physics* Taylor & Francis (2009).

[16] H. H. Wensik and H. Löwen, Phys. Rev. Letters **97**, 038303 (2006).

[17] Th. Kirchhof, H. Löwen, R. Klein, Phys. Rev. E **53**, 5 (1996).

[18] C. A. Mirkin, R. L. Letsinger, R. C. Mucic and J. J. Storhoff, Nature, **382**, 607 (1996).

[19] D. Nykypanchuk, M. M. Maye, D. van der Lelie and O. Gang, Nature, **451**, 549 (2008).

[20] Kyle J. M. Bishop, Christopher E. Wilmer, Siowling Soh, and Bartosz A. Grzybowski, small **5**, 14 (2009).

[21] A. P. Alivisatos, K. P. Johnsson, X. G. Peng, T. E. Wilson, C. J. Loweth, M. P. Bruchez Jr and P. G. Schultz, Nature, **382**, 609 (1996).

[22] A. van Blaaderen, Nature, **439**, 545 (2006).

[23] A. B. Pawar and I. Kretzschmar, Langmuir, **24**, 355 (2009).

[24] Emanuela Bianchi, Ronald Blaak and Christos N. Likos, Phys. Chem. Phys., **13**, 6397?6410 (2011).

[25] Y. H. Liu, L. Y. Chew, and M. Y. Yu, Phys. Rev. E **78**, 066405 (2008).

[26] T. Chou and David R. Nelson, Phys. Rev. E **48**, 6 (1993).

[27] Hongbao Xin, Rui Xu, Baojun Li, Scientific Reports **2**, 818 (2012).

[28] L. Q. Costa Campos, S. W. S. Apolinario, H. Löwen, Phys. Rev. E **88**, 042313 (2013).

[29] Katherlne J. Strandburg, Rev. Mod. Phys **60**, No. 1 (1988).

[30] Kosterlitz, J. M., and D. J. Thouless, J. Phys. C **6**, 1181 (1973).

[31] Halperin, B. I., and D. R. Nelson, Phys. Rev. Lett. **41**, 121 (1978).

[32] Young, A. P., Phys. Rev. B **19**, 1855 (1979).

[33] Mermin, N. D., and H. Wagner, Phys. Rev. Lett. **17**, 1133 (1966).

[34] Urs Gasser, Christoph Eisenmann, Georg Maret, and Peter Keim, ChemPhysChem **11**, 963-970 (2010).

[35] A. Jaster, Phys. Rev. E **59**, 3 (1999).

[36] Etienne P. Bernard and Werner Krauth, PRL **107**, 155704 (2011).

[37] Sven Deutschländer, Tobias Horn, Hartmut Löwen, Georg Maret, and Peter Keim, PRL **111**, 098301 (2013).

[38] Sebastian C. Kapfer and Werner Krauth, PRL **114**, 035702 (2015).

[39] Alice L. Thorneywork, Joshua L. Abbott, Dirk G. A. L. Aarts, and Roel P. A. Dullens, PRL **118**, 158001 (2017).

[40] Thomas A. Weber, Frank H. Stilinger, Phys. Rev. E **48**, 6 (1993).

[41] P. Bladon and D. Frenkel, Phys. Rev. Lett. **74**, 2519 (1995).

[42] A. H. Marcus and S. A. Rice, Phys. Rev. E **55**, 637 (1997).

[43] Pallop Karnchanaphanurach, Binhua Lin, and Stuart A. Rice, Phys. Rev. E **61**, 4 (2000).

[44] Di Du, Manolis Doxastakis, Elaa Hilou and Sibani Lisa Biswal, Soft Matter **13**, 1548 (2017).

[45] C. Reichhardt and C. J. Olson Reichhardt, Phys. Rev. Letters **92**, 10 (2004).

[46] S. W. S. Apolinario and F. M. Peeters, Phys. Rev. B **78**, 024202 (2008).

[47] S. W. S. Apolinario and F. M. Peeters, Phys. Rev. E. **76** 031107 (2007).

[48] S. W. S. Apolinario, J. Albino Aguiar, and F. M. Peeters, Phys. Rev. E **90**, 063113 (2014).

[49] S. W. S. Apolinario, B. Partoens, and F. M. Peeters, Phys. Rev. E **74**, 031107 (2006).

[50] Y. Peng, Z.-R. Wang, A. M. Alsayed, A. G. Yodh, Y. Han, Phys. Rev. E **83**, 011404 (2011).

[51] Sayuri Tanaka, Yuma Oki, and Yasuyuki Kimura, Phys. Rev. E **89**, 052305 (2014).

[52] Arunas Radzvilavivius, Phys. Rev. E, **86**, 051111 (2012).

[53] D. C. Rapaport, *The Art of Molecular Dynamics Simulation*, Cambridge University Press, 2004.

[54] A. Ivlev, H. Lwen, G. Morfill, and C. P. Royall, *Complex Plasmas and Colloidal Dispersions: Particle-resolved Studies of Classical Liquids and Solids.*, Series in Soft Condensed Matter, Vol. 5 (World Scientific, Singapore, 2012).

[55] Hiroshi Noguchi, Phys. Rev. E **93**, 0542404 (2016).

[56] Keola Wierschem and Efstratios Manousakis, Phys. Rev. B **83**, 214108 (2011).

[57] K. Koperwas, F. Affouard, J. Gerges, L.-C. Valdes, K. Adrjanowicz, and M. Paluch, Phys. Rev. B, **96**, 224106 (2017).

[58] J. C. N. Carvalho, W. P. Ferreira, G. A. Farias, and F. M. Peeters, Phys. Rev. B **83**, 094109 (2011).

[59] L. Q. C. Campos, C. C. S. Silva, and S. W. S. Apolinario, Phys. Rev. E 86, 051402 (2012).

[60] Hiroo Totsuji, Chieko Totsuji, and Kenji Tsuruta, Phys. Rev. E. **64**, 066402 (2001).

[61] Ming-Tzo Wei and Arthur Chiou , Opt. Express **13**, Issue 15, pp. 5798-5806 (2005).

[62] Ming-Tzo Wei, Angela Zaorski, Huseyin C. Yalcin, Jing Wang, Melissa Hallow, Samir N. Ghadiali, Arthur Chiou, and H. Daniel Ou-Yang, Opt. Express **16**, Issue 12, pp. 8594-8603 (2008).

[63] David. P. Landau, Kurt Binder, *A Guide to Monte Carlo Simulation in Statistical Physics.*, Cambridge University Press, 2000.

[64] L. Q. Costa Campos, S. W. S. Apolinario, Phys. Rev. E **91**, 012305 (2015).

[65] H.Gould, J. Tobochnik, and W. Christian. *An introduction to computer simulations methods: applications to physical systems.* Addison-Wesley Pearson, 2007.

[66] Jigar K. Mistry, Ameya M. Natu, Michael R. Van De Mark, J. Appl Polym. Sci **131**, 40916 (2014).

[67] Adam M. Becker, Robert M. Ziff, Phys. Rev. E **80**, 041101 (2009).

[68] E. Dubois-Violette, P. Pieranski, F. Rothen and L. Strzelecki, J. Physique **41**, 369-376 (1980).

[69] J. P. Mithen, A. J. Callison, and R. P. Sear, The Journal Of Chemical Physics **142**, 224505 (2015).

[70] Caroline Desgranges and Jerome Delhommelle, J. AM. CHEM. SOC. **128**, 47, (2006).